IEEE Access
Multidisciplinary ⋮ Rapid Review ⋮ Open Access Journal

Received 7 May 2024, accepted 23 May 2024, date of publication 27 May 2024, date of current version 5 June 2024.

Digital Object Identifier 10.1109/ACCESS.2024.3405994

RESEARCH ARTICLE

A Hybrid Controlling Parameters of Power System Stabilizer and Virtual Inertia Using Harris Hawk Optimizer in Interconnected Renewable Power Systems

MOHAMAD ALMAS PRAKASA[1], IMAM ROBANDI[1], RYO NISHIMURA[2], AND MUHAMMAD RUSWANDI DJALAL[1]

[1]Department of Electrical Engineering, Institut Teknologi Sepuluh Nopember, Surabaya 60111, Indonesia
[2]Department of Information and Electronics, Faculty of Engineering, Tottori University, Tottori 680-8552, Japan

Corresponding author: Imam Robandi (robandi@ee.its.ac.id)

This work was sponsored by the Directorate of Research and Community Service (Direktorat Riset, Teknologi, dan Pengabdian kepada Masyarakat, DRPM), Ministry of Education, Culture, Research, and Technology (Kementerian Pendidikan, Kebudayaan, Riset dan Teknologi, Kemendikbudristek) of the Republic of Indonesia under grant 1457/PKS/ITS/2024.

ABSTRACT A hybrid controlling method for stability controllers is needed in the interconnected renewable power systems due to the working conditions being diverse from low to high levels of Renewable Energy Sources (RES). Power System Stabilizer and Virtual Inertia (PSS-VI) are viable to provide a wider enhancement effect in the stability. This paper proposes a new approach to enhance the stability of interconnected renewable power systems by hybrid controlling parameters of PSS-VI. A robust optimizer based on Harris Hawk Optimizer (HHO) is formulated. Interconnected renewable power systems are modeled based on multi-area power systems with different energy resources, including conventional generators, Solar Power Generation (SPG), and Wind Power Generation (WPG). Besides that, the Battery Storage System (BSS) is also dispatched to realize the virtual inertia emulation. The optimal parameters by HHO are compared with the other recent novel algorithms. The optimal controlling parameters of PSS-VI by HHO in interconnected renewable power systems performed in low to high RES conditions. Based on the convergence curve analysis, HHO conducts the best fitness value with faster iterations than the compared algorithm. The results of hybrid controlling parameters by HHO can significantly suppress the Rate of Change of Frequency (RoCoF) by 5.99% and 4.89% in low-RES and high-RES conditions, respectively. Moreover, the hybrid controlling parameters for PSS-VI offer smoother response and transition in frequency and inter-area power exchange responses.

INDEX TERMS Harris Hawk Optimizer, interconnected power system, power system stabilizer, renewable energy sources, virtual inertia.

NOMENCLATURE

A	WT's swept area.
C_P	WT's power coefficient.
D	Damping properties.
D_{VI}	Additional damping properties.
E	Escaping energy of the rabbit in HHO.
E_{boc}	Open-circuit voltage in BSS.
E_{b1}	Overvoltage tolerance in BSS.
E_{fd}	Exciter's voltage.
E'_q	Terminal voltage in the generator.
E_o	The initial energy of the rabbit in HHO.
$G_{SPG}(s)$	The transfer function for SPG.
$G_{WPG}(s)$	The transfer function for WPG.
N_{PV}	Power rating of the PV system.
P_{BSS}	Power output from BSS.

The associate editor coordinating the review of this manuscript and approving it for publication was Nga Nguyen.

P_{INV_max}	Maximum value of inverter's filter.
P_{INV_min}	Minimum value of inverter's filter.
P_{VI}	Inertia power emulation.
q	A random value between 0 to 1 that determines the hawk's position.
r	Rabbit's probability of escaping.
r_{bp}	Self-discharge resistance.
r_{bs}	Internal tolerance in BSS.
R_{VI}	Inertia droop.
r_1, r_2, r_3, r_4, r_5	Randomly generated numbers between 0 to 1 in HHO.
T	Ambient temperature.
t	The current iteration in HHO.
T_A	Amplifier's time response.
T_b	BSS's time response.
T'_{do}	Exciter's time constant.
T_e	Electrical torque areas.
T_{INV}	Inverter's time response.
T_{jk}	Synchronization coefficient between two areas.
t_{max}	Maximum iteration in HHO.
T_S	Temperature in standard test condition.
T_{SPG}	SPG's time constant.
T_W	Washed-out constant.
T_{WPG}	WPG's time constant.
T_1, T_2, T_3, T_4	Tunable parameters in PSS.
ub	Upper bound.
V_{PSS}	Signal output from PSS.
X_{CO}	Reactance in BSS.
H	Inertia properties.
I_{O_BSS}	DC in BSS.
J	Jump strength of the rabbit in HHO.
k_A	Amplifier's gain constant.
K_b	BSS's gain control.
K_{PSS}	PSS's gain constant.
K_{SPG}	SPG's gain constant.
K_{VI}	Virtual inertia properties.
K_{WPG}	WPG's gain constant.
$K_1 - K_6$	Heffron-Phillips' constants.
lb	The lower bound of search space.
N	Number of population in HHO.
X_i	Initial position of hawks.
$X_m(t)$	Average position of hawks.
X_{rabbit}	Rabbit vector in HHO.
$X_{rabbit}(t)$	The current rabbit's location.
$X_r(t)$	Random movement of a hawk.
$X(t)$	Current position of a hawk.
$X(t+1)$	Hawk's position.
α_T	Temperature coefficient.
ΔE_{bt}	Terminal equivalent.
ΔE_{CO}	Non-overlapping voltage in DC.
ΔE_d	Damping signal in VI.
Δf	Frequency deviation.
Δf_1	Frequency response in Area 1.
Δf_2	Frequency response in Area 2.
ΔP_L	Change in power load.
ΔP_{SPG}	Change in solar power output.
$\Delta P_{tie,j}$	Exchange power via tie-line.
$\Delta P_{tie,jk}$	Tie-line power exchange between j and k.
ΔP_{WT}	Change in wind turbine output.
ΔV_{Wind}	Change in wind speed.
$\Delta X(t)$	Average distance between the hawks and the rabbit.
$\Delta\delta$	Power angle deviation.
ρ	Air density coefficient.
$\Delta\phi$	Change in solar GHI level.
$\Delta\omega$	Rotor speed deviation.
ϕ_S	Solar GHI level in the standard test condition.
ω_r	Rotor speed.

LIST OF ABBREVIATIONS

AOA	Arithmetic Optimizer Algorithm.
AVR	Automatic Voltage Regulator.
BSS	Battery Storage System.
CDI	Comprehensive Damping Index.
DI-PSS	Dual Input Power System Stabilizer.
EOA	Equilibrium Optimizer Algorithm.
ESS	Energy Storage System.
FLC	Fuzzy Logic Controller.
GHI	Global Horizontal Irradiation.
HHO	Harris Hawk Optimizer.
HVDC	High Voltage Direct Current.
LF	Levy Flight.
LQG	Linear Quadratic Gaussian.
LQI	Linear Quadratic Integral.
LQR	Linear Quadratic Regulator.
MFO	Moth Flame Optimizer.
MOA	Mayfly Optimizer Algorithm.
MRFA	Manta Ray Foraging Algorithm.
PI	Proportional-Integral (Controller).
POD	Power Oscillation Damping.
PSS	Power System Stabilizer.
PSS-VI	A combination of PSS and VI.
PV	Photovoltaic.
RES	Renewable Energy Sources.
RoCoF	Rate of Change of Frequency.
RSO	Rat Swarm Optimizer.
SMIB	Single Machine Infinite Bus.
SPG	Solar Power Generation.
SSSC	Static Series Synchronous Compensator.
STATCOM	Static Synchronous Compensator.
SVC	Static Var Compensator.
VI	Virtual Inertia.
WECC	Western Electricity Coordinating Council.
WOA	Whale Optimizer Algorithm.
WPG	Wind Power Generation.
WT	Wind Turbine.

I. INTRODUCTION

A shifting trend from centralized power generation systems towards decentralized power generation systems is inevitable [1]. A decentralized power generation system

offers a more economical and flexible way of maintaining reliability and feasibility than centralized ones [2]. Moreover, a decentralized power generation system can be built on a wider scale, such as from small-scale to large-scale power generation systems. This condition opens the opportunity for the user to deploy their own power or energy systems [3]. This kind of power generation system is popularly known as a microgrid power system.

A microgrid power system offers flexibility in the power generation of resources [4]. Microgrids can utilize the potential Renewable Energy Sources (RES) in different specific sites. For example, Solar Power Generation (SPG) based on Photovoltaic (PV) technology can be dispatched to sites with sufficient solar Global Horizontal Irradiation (GHI) with long duration of sunlight. Another example is the small-scale Wind Power Generation (WPG) based on Wind Turbine (WT) technology that is dispatched on windy sites. However, RES power fluctuation that depends on uncertain natural conditions becoming a challenge in the continuity of electricity supply [5]. Thus, microgrids usually use hybrid generation resources. Moreover, the Energy Storage System (ESS) is usually dispatched to ensure the continuity of power supply [6].

The microgrids can be connected to form an interconnected renewable power system [7], [8]. In this form, each system can support the other if there is a lack of power electricity supply. Besides the advantages, this form has crucial problems. One of the problems is that dynamic stability is more inferred [9]. Moreover, the RES energy transfer in interconnected power systems worsens this condition. In dynamic stability study, these kinds of disturbances must mitigated quickly with proper approaches [10]. If it is not, then the oscillations can spread throughout the areas and cause blackouts.

In a power system without RES generators, stability is maintained with controllers that have specific effects on the power system [11]. A Power System Stabilizer (PSS) is usually established as an important controller. The power system with PSS can tackle the small-signal oscillation (usually occurs in 0.1 to 3 Hz) effectively [12]. The PSS still exists due to its instant effect to enhance dynamic stability [13]. PSS performance in enhancing stability is dependent on controlling parameters that must be tuned optimally. These controlling parameters produce a signal to trigger the exciter and the Automatic Voltage Regulator (AVR) adjusts the electrical torque to dampen the oscillation. In more complex power systems, PSS is usually combined with other controllers to work complementary. For example, in [10], the controlling parameters of PSS with the Static Var Compensator (SVC) using the Mayfly Optimizer Algorithm (MOA) is implemented for Indonesia's real power system. In [14], PSS is coordinated with SVC and the other supplementary damping controllers using deep and reinforcement learning algorithms in High Voltage Direct Current (HVDC) power systems. In [15] and [16], the controlling parameters of PSS are also combined with the other controllers, like Static Synchronous Compensator (STATCOM), Static Series Synchronous Compensator (SSSC), etc.

On the other hand, the stability challenge in renewable power systems become more crucial [17]. It is caused by the renewable generators being considered inverter-based with power electronic components. This system does not contain the damping and inertia like in conventional power systems. Due to PSS being related to mechanical parts in generators, it makes the PSS is no longer effectively to be implemented in power systems that integrated with RES. Thus, the Virtual Inertia (VI) concept appeared as a viable solution [18]. VI scheme has been implemented in islanded, grid-connected, and interconnected power systems with low to high levels of RES [19], [20], [21]. VI can imitate the damping and inertia properties in RES generators by regulating the Energy Storage System (ESS) and inverter working behavior with the proper controlling scheme. VI emulation is also related to tunable parameters that must be controlled optimally. The proper parameters can trigger the ESS and inverter to suppress the Rate of Change of Frequency (RoCoF) of the system and reduce the frequency nadir.

Both PSS and VI need their tunable parameter to be controlled optimally, thus various methods have been developed. The first group is predictive-based methods, like Linear Quadratic Regulator (LQR), Linear Quadratic Integral (LQI), and Linear Quadratic Gaussian (LQG) [22], [32], [33]. The H∞ control method has also been conducted [19], [34]. Besides that, Fuzzy Logic Controller (FLC)-based control is also popular in PSS or VI cases [16], [25]. The next group is intelligent algorithms based on learning algorithms, like Machine Learning, Deep Learning, Reinforcement Learning, etc [14], [26], [35]. Besides that, the most popular group is intelligent optimizers based on metaheuristic algorithms, such as the Whale Optimizer Algorithm (WOA) [21], Mayfly Optimizer Algorithm (MOA) [10], Manta Ray Foraging Algorithm (MRFA) [36], Equilibrium Optimizer Algorithm (EOA) [37], Arithmetic Optimizer Algorithm (AOA) [8], Moth Flame Optimizer (MFO) [38], Rat Swarm Optimizer (RSO) [30], Harris Hawk Optimizer (HHO) [39], etc. Intelligent optimizers based on metaheuristic algorithms offer convenience and flexibility in exploring and exploiting the best results. Unlike the others, metaheuristic algorithms are not dependent on specific rules and are not limited to learning datasets. Harris Hawk Optimizer (HHO) has arisen as a popular recent algorithm due to its unique robustness in the exploration and exploitation process [40]. HHO, inspired by the unique behavior of the Harris Hawk hunting schemes, has been proven to solve various cases in the world [41], [42].

The summary of existing literature related to dynamic stability enhancement is stated in Table 1. The majority of previous have discussed the PSS combination with other controllers. The summary of existing literature related to dynamic stability enhancement is stated in Table 1. The majority of previous have discussed the PSS combination

with other controllers. The latest literature investigated that PSS and VI can be combined as a viable solution to maintain dynamic stability in wide levels of RES [31]. The PSS and VI have been proven correlated in theoretical and simulation approaches. The PSS and VI have complement behavior in improving dynamic stability. The PSS is more effective in low-RES conditions. Meanwhile, VI is more effective in high-RES conditions. Moreover, the proper combination of PSS and VI better dynamic stability improvement in the wider range of RES-level conditions compared to individual components. However, the investigation is conducted only in a microgrid power system. Thus, further investigation into the interconnected renewable power systems is needed. The complex problem in interconnected renewable power systems motivates this work to extend the investigation regarding the hybrid controlling parameters of PSS and VI (PSS-VI). The significant contribution and impact of this work of this paper are listed in the following:

1) Proposing a new approach for enhancing the stability of interconnected renewable power systems by performing the hybrid controlling parameters of PSS-VI using HHO as a robust optimizer.
2) Giving the detailed dynamic model of the interconnected renewable power systems for the implementation of PSS-VI. The proposed system consists of Solar Power Generation (SPG) and Wind Power Generation (WPG). and Battery Storage System (BSS) to realize the virtual inertia emulation.
3) Demonstrating a wider enhancement effect to adapt in various dynamic behaviors when a disturbance occurs in different RES levels by hybrid controlling of PSS-VI.

This paper is arranged as follows: In Section II, the interconnected renewable power systems model are described. In Section III, the proposed hybrid controlling parameter method for PSS-VI is presented. In Section IV, the investigation results are discussed, including a comparison with the other methods, and a deep analysis of interconnected renewable power system behavior. In the rest, the significant contribution of this work is concluded in Section V.

II. SYSTEM MODEL

The investigated interconnected renewable power systems are illustrated in Figure 1. The system consists of two area power systems with different RES connected via tie-lines to provide a power exchange feature. The mathematical models for the dynamic behavior of each component are presented. Then, the illustration and state-space equations of an interconnected renewable power system are also designed. Besides that, the PSS and VI emulation schemes are also described.

A. CONVENTIONAL GENERATOR MODEL

In this paper, the Linearized Heffron-Phillips Model for power systems is used. This model is appropriate for simulating the dynamic behavior in the power generator, including the governor and turbine, excitation and AVR, and the built-in effect of the PSS. The Linearized Heffron-Phillips in a mathematical model is given by Equation (1) until Equation (4) [43].

$$\Delta\dot{\delta} = \omega_r \Delta\omega \tag{1}$$

$$\Delta\dot{\omega} = -\frac{K_1}{2H}\Delta\delta - \frac{D}{2H}\Delta\omega - \frac{K_2}{2H}E'_q \tag{2}$$

$$\Delta\dot{E}'_q = \frac{K_4}{T'_{do}}\Delta\delta - \frac{\Delta E'_q}{T'_{do}K_3} + \frac{E_{fd}}{T'_{do}} \tag{3}$$

$$\Delta\dot{E}'_{fd} = -\frac{k_A K_5}{T_A}\Delta\delta - \frac{k_A K_6}{T_A}\Delta E'_q - \frac{E_{fd}}{T_A} + \frac{k_A}{T_A}\Delta V_{PSS} \tag{4}$$

with $\Delta\delta$ is power angle deviation, ω_r is rotor speed, and $\Delta\omega$ is rotor speed deviation that is proportional to frequency deviation (Δf). H and D are defined as the inertia and damping properties of the power system, respectively. E'_q is terminal voltage in the generator, T'_{do} exciter's time constant, E_{fd} is the exciter's voltage, k_A is the amplifier's gain constant, T_A is the amplifier's time response. K_1 until K_6 are additional Heffron-Phillips' constants representing the connection between components.

B. SPG AND WPG MODEL

Based on [23] and [24], the simplified low-order model for RES is adequate for dynamic stability investigation. Solar Power Generation (SPG) is defined as Equation (5) [44].

$$G_{SPG}(s) = \frac{K_{SPG}}{1 + sT_{SPG}} = \frac{\Delta P_{SPG}}{\Delta\phi} \tag{5}$$

with K_{SPG} and T_{SPG} are SPG gain constant and time constant, respectively. ΔP_{SPG} is a change in solar power output based on Equation (6) and $\Delta\phi$ is a change in solar irradiance level.

$$\Delta P_{SPG} = N_{PV} \times \left(\frac{\phi}{\phi_S}\right) \times [1 + \alpha_T(T - T_S)] \times \eta \tag{6}$$

with N_{PV} is the power rating of the PV system in SPG. ϕ and ϕ_S is the solar irradiance level in the current condition and the standard test condition, respectively. Meanwhile, α_T, T, and T_S are temperature coefficient, ambient temperature, and temperature in standard test conditions of the PV system, respectively. In this paper, ΔP_{SPG} is assumed linearly affected by $\Delta\phi$ only.

Besides that, Wind Power Generation (WPG) is defined as Equation (7) [45].

$$G_{WPG}(s) = \frac{K_{WPG}}{1 + sT_{WPG}} = \frac{\Delta P_{WPG}}{\Delta V_{Wind}} \tag{7}$$

with K_{WPG} and T_{WPG} are WPG gain constant and time constant, respectively. ΔP_{WT} is a change in WT output based on Equation (8) and ΔV_{Wind} is a change in wind speed.

$$\Delta P_{WPG} = \frac{1}{2}\rho A C_p V^3_{Wind} \tag{8}$$

with ρ is air density coefficient, A is WT's swept area, C_P is WT's power coefficient, and V_{wind} is the wind speed levels. In this paper, ΔP_{WPG} is assumed linearly affected by ΔV_{Wind} only.

TABLE 1. Summary of existing literatures.

Ref.	Investigated System	Proposed Controller	Algorithm	Remarks
[22]	Single Machine Infinite Bus (SMIB)	State feedback	LQR via metaheuristic	
[23]	High-penetration microgrid with thermal plant, PV, WT, and ESS	VI	Derivative technique	A complex model and formulation are needed for proper implementation
[24]	Islanded microgrid with thermal power plant, PV, WT, and ESS	VI	H∞ and PI controller	
[16]	Two machines-based system	PSS-STATCOM	FLC	Pre-determined rules should be defined with proper consideration and the relative between users can be confused
[25]	The 3-machine 9-node system with WT	VI	FLC	
[14]	Western Electricity Coordinating Council (WECC) system	Wide-Area Damping Controller	Deep Neural Network	The learning-based algorithm needs specific datasets to ensure the learning process becomes accurate
[26]	Isolated microgrid with high penetration of PV and WT	VI	Reinforcement Learning	
[21]	High-penetration renewable power systems	VI	WOA	The investigation only considered high-penetration condition
[27]	Interconnected power system with PV and retired BESS	VI	FA	The investigations only used the common metaheuristic algorithms
[28]	Interconnected power system with PV system and Capacitor-based ESS	VI	PSO	
[10]	The interconnected power system in Sulselrabar Electricity System, Indonesia	Hybrid multi-band PSS-SVC	MOA	
[29]	New England system and the two-area symmetrical system	Hybrid PSS-SSSCPOD	MOA	The hybrid controllers were proposed for power systems without RES
[30]	Conventional interconnected two-area power system	Hybrid Conventional PSS-SVC	RSO	
[31]	Renewable microgrid power system: PV, WT, and BSS	Hybrid PSS-VI	HHO	The investigated system only consists of a single-area microgrid
Current Work	**Interconnected renewable power systems: conventional generators, SPG, WPG, and BSS**	**Hybrid PSS-VI**	**HHO**	**Enhancing the stability of interconnected renewable power systems by the hybrid controlling parameters of PSS-VI**

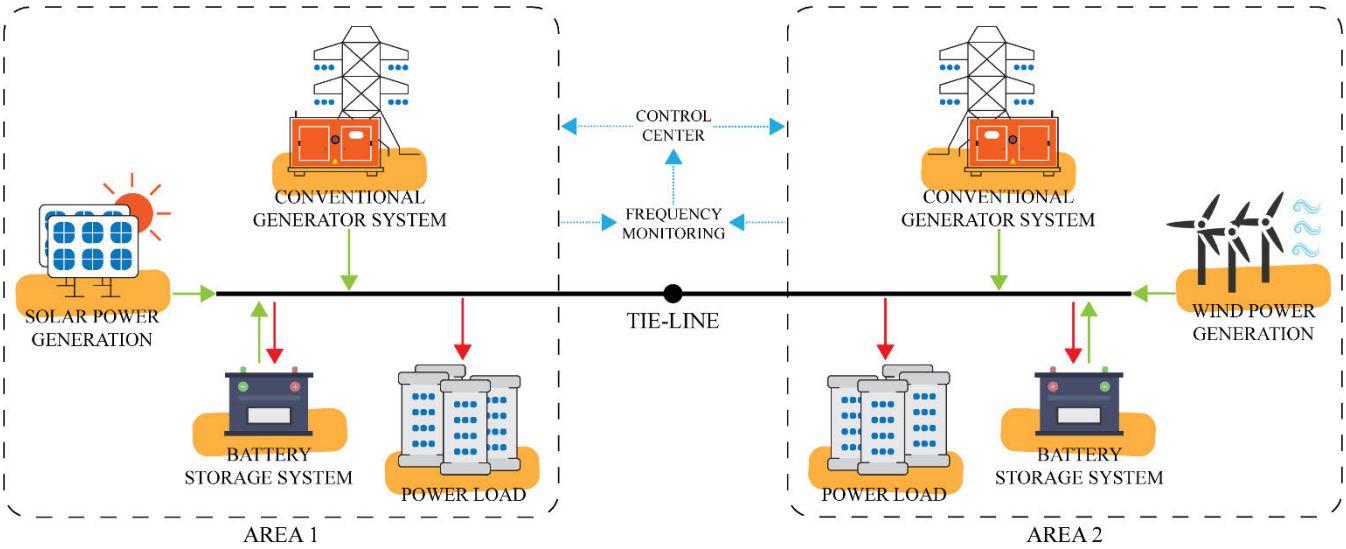

FIGURE 1. Synoptic diagram for interconnected renewable power systems.

C. PSS MODEL

The dynamic enhancement by PSS is related to the electrical loop in the generator [11], [13], [46]. This paper uses Dual-Input PSS (DI-PSS) with Δf and $\Delta\delta$ as input signals. PSS injects an additional voltage signal (V_{PSS}) into the excitation system. It triggers the system to adjust magnetic flux

that produces electrical torque (T_e) proportional to Δf and $\Delta\delta$. Adjustment in T_e can dampen the small-signal oscillation when a disturbance occurs. In general, the PSS dynamic equation is described as Equation (9).

$$V_{PSS} = K_{PSS}\left[\frac{sT_w}{1+sT_w}\right]\left[\frac{(1+T_1 s)}{(1+T_2 s)}\frac{(1+T_3 s)}{(1+T_4 s)}\right]\Delta f \quad (9)$$

with K_{PSS} is PSS's gain constant, T_W is the washed-out constant, and T_1, T_2, T_3, and T_4 are the tunable parameters for adjusting the signal reference into the excitation system.

The DI-PSS is conducted in Figure 2 [46]. DI-PSS has three gain constants. K_{PSS1} is tunable. Meanwhile, K_{PSS2} and K_{PSS3} are determined by $T_7/2H$ and 1, respectively. DI-PSS has four washed-out blocks. T_{W1}, T_{W2},and T_{W3} with a default parameter of 10. T_{W4} is usually bypassed. It has also four control time parameters: $T_6 = 0$, $T_7 = T_{W2}$, $T_8 = 0.3$, and $T_9 = 0.15$. DI-PSS has a special feature, ramp-tracking, that is defined as $M = 2$ and $N = 4$.

D. VI AND BSS MODEL

The damping and inertia properties can be emulated in RES generators by controlling the BSS and inverter behavior with the proper scheme [27], [47]. The VI emulation scheme with BSS and inverter is illustrated in Figure 3. It takes Δf as an input signal. In VI concept, Δf is defined as Rate of Change of Frequency (RoCoF). The RoCoF is calculated to give the reference into the system for the amount of inertia power emulation (P_{VI}) needed to enhance the dynamic stability when a disturbance occurs as given by Equation (10).

$$P_{VI} = \frac{sK_{VI} + D_{VI}}{1+sT_{INV}}\left(\frac{\Delta f}{R_{VI}}\right) \quad (10)$$

with K_{VI} is virtual inertia properties, D_{VI} is additional damping properties, T_{INV} is the inverter's time response, and R_{VI} is inertia droop.

From Figure 3, it can be seen that the VI control scheme is connected with BSS. In this paper, the BSS model is focused on injecting active power within a short time. BSS relation with the damping signal (ΔE_d) is defined by Equation (11).

$$\Delta E_d = \frac{K_b}{1+sT_b}\Delta f \quad (11)$$

with K_b is the gain control and T_b is the battery's time response. I_{O_BSS} is direct current, ΔE_{CO} is non-overlapping voltage in direct current, X_{CO} is reactance, ΔE_{bt} is terminal equivalent, E_{b1} is overvoltage tolerance, E_{boc} is open-circuit voltage, r_{bs} is internal resistance, r_{bp} is self-discharge resistance, and r_{b1} is overvoltage resistance.

Power output from BSS (P_{BSS}) is forwarded through the inverter. The inverter regulates the power with the block of inverter time response (T_{INV}) and filter (P_{INV_max} and P_{INV_min}). Then, the properly regulated P_{VI} can be injected into the system for dynamic stability enhancement.

E. INTERCONNECTED RENEWABLE POWER SYSTEMS

The interconnected renewable power system is constructed as in Figure 4. The dynamic behavior equations in the power exchange via tie-line ($\Delta P_{tie,j}$) is given by Equation (12) and Equation (13) [18], [48].

$$\Delta P_{tie,j}(s) = \sum_{\substack{j=1\\ j\neq k}}^{y} \Delta P_{tie,jk}(s) \quad (12)$$

$$\Delta P_{tie,j}(s) = \frac{2\pi}{s}\left[\sum_{\substack{j=1\\ j\neq k}}^{y} T_{jk}\Delta f_j - \sum_{\substack{j=1\\ j\neq k}}^{y} T_{jk}\Delta f_k\right] \quad (13)$$

with T_{jk} is the synchronization coefficient between two areas. $\Delta P_{tie,jk}$ is the tie-line power exchange between j and k.

In Area 1, power generation consists of a combination of conventional generators and SPG. Meanwhile, in Area 2, the power generation consists of a hybrid of conventional generators and WPG. Each RES generation is assumed to be connected to an ideal power inverter. Each area has BSS to realize the virtual inertia emulation. Each area has also different power load (ΔP_L) characteristics. PSS and VI controllers are dispatched as additional controllers to maintain the dynamic stability of the system.

In this paper, the mathematical model of an interconnected renewable power system is built based on the frequency regulation model of the power system. This system conducts a frequency monitoring system to collect stability references from each area. The measured frequencies are calculated through the control center. Then, the control system throws feedback control signals for adjusting PSS-VI parameters in each area. Thus, the dynamic behavior is indicated by the frequency response of each system. The relation between frequency response and components in Area 1 (Δf_1) is shown in Equation (14).

$$\Delta f_1(s) = \frac{1}{2H_1 s + D_1}\left[\Delta P_{m1}(s) + \Delta P_{SPG}(s) + \Delta P_{VI1}(s) - \Delta P_{L1}(s) - \Delta P_{tie,12}(s)\right] \quad (14)$$

Besides that, the relation between frequency response and components in Area 2 (Δf_2) is shown in Equation (15).

$$\Delta f_2(s) = \frac{1}{2H_2 s + D_2}\left[\Delta P_{m2}(s) + (\Delta P_{WPG}(s) + \Delta P_{VI2}(s) - \Delta P_{L2}(s) - \Delta P_{tie,21}(s)\right] \quad (15)$$

In dynamic stability analysis, the state-space model is needed to make the in-depth investigation becomes easier. A general representation of the state-space model for modern power systems is given by Equation (16).

$$\dot{x} = Ax + B_1 w + B_2 u \quad (16)$$

In this paper, by constituting the dynamic equation of each component, the state-space model for interconnected renewable power systems is given by Equation (17) until Equation (21).

$$x^T = [x_1 x_2] \quad (17)$$

$$x_1 = [\Delta f_1 \Delta\delta_1 \Delta P_{m1} \Delta P_{SPG} \Delta P_{tie,12} \Delta P_{VI1} \Delta V_{PSS1}] \quad (18)$$

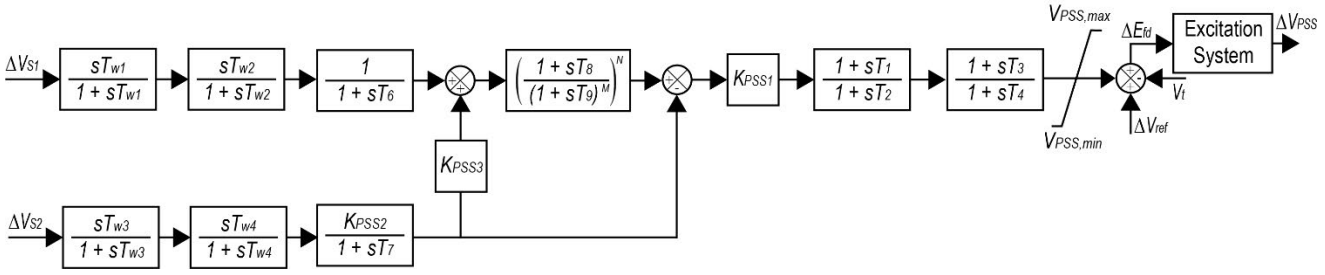

FIGURE 2. Block diagram for DI-PSS.

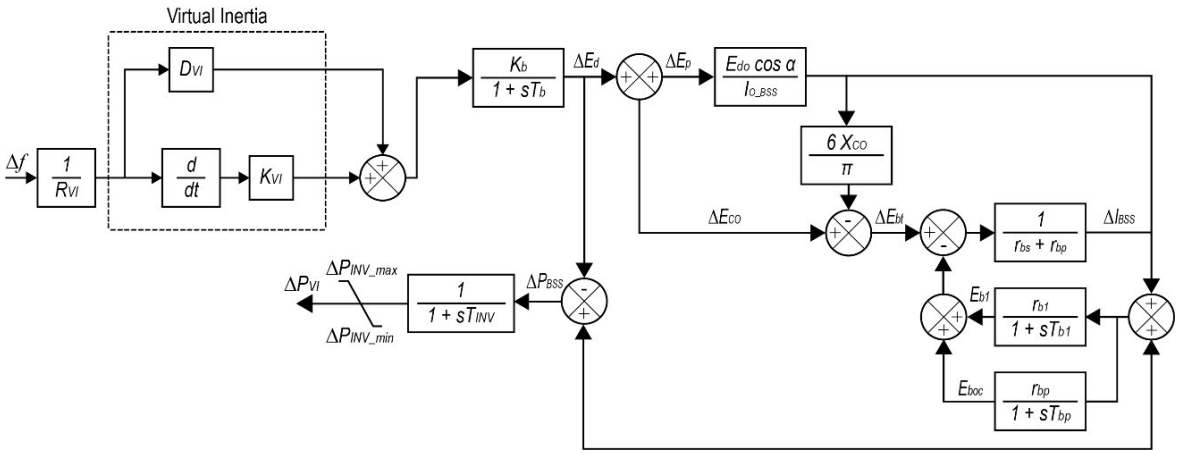

FIGURE 3. Block diagram for VI emulation scheme with BSS.

$$x_2 = [\Delta f_2 \Delta\delta_2 \Delta P_{m2} \Delta P_{WPG} \Delta P_{tie,21} \Delta P_{VI2} \Delta V_{PSS2}] \quad (19)$$

$$x^T = [\Delta P_{L1} \Delta P_{L2} \Delta\phi \Delta V_{Wind}] \quad (20)$$

$$u^T = [\frac{d\Delta f_1}{dt} \frac{d\Delta f_2}{dt}] \quad (21)$$

with x defined as the observed variable matrix, w determined as the input for small-signal disturbance, and u represented as the control input signal for PSS or VI controllers.

III. PROPOSED METHOD IN HYBRID CONTROLLING PARAMETER FOR PSS-VI

In this section, the problem formulation of the hybrid controlling parameter for PSS-VI is described. Then, the proposed PSS-VI optimizer based on HHO is explained in a detailed flowchart with steps.

A. PROBLEM FORMULATION

In dynamic stability study, the stability of the power system can be investigated using eigenvalue analysis. The eigenvalue analysis is conducted by calculating the determinant of matrix A in Equation (16) which represents the condition of the system. The eigenvalue component of matrix A is given by Equation (22).

$$\lambda_A = \sigma_A + j\omega_A \quad (22)$$

with σ is the real part of the eigenvalue representing the damping property of the system and ω is the imaginary part of the eigenvalue representing the oscillation. The Δf is related to ω as in Equation (23).

$$f = \frac{\omega}{2\pi} \quad (23)$$

It can be obtained the damping ratio or Comprehensive Damping Index (CDI) of the system as in Equation (24).

$$\xi_A = \frac{-\sigma_A}{\sqrt{\sigma_A^2 + j\omega_A^2}} \quad (24)$$

The objective function formulation in the hybrid controlling parameter for PSS-VI is to maximize the CDI as given in Equation (25).

$$CDI = \sum_{t=1}^{n} (1 - \xi_A) \quad (25)$$

with t is the time variable from 1 second until n time simulation.

The CDI value is influenced by the optimal parameters of PSS-VI. Thus, the tunable parameters in PSS-VI are defined as control variables. The control variables are bounded by Equation (26) until Equation (32).

$$K_{PSS1,min\,a} \le K_{PSS1\,a} \le K_{PSS1,max\,a} \quad (26)$$

$$T_{1min\,a} \le T_{1\,a} \le T_{1,max\,a} \quad (27)$$

$$T_{2min\,a} \le T_{2\,a} \le T_{2,max\,a} \quad (28)$$

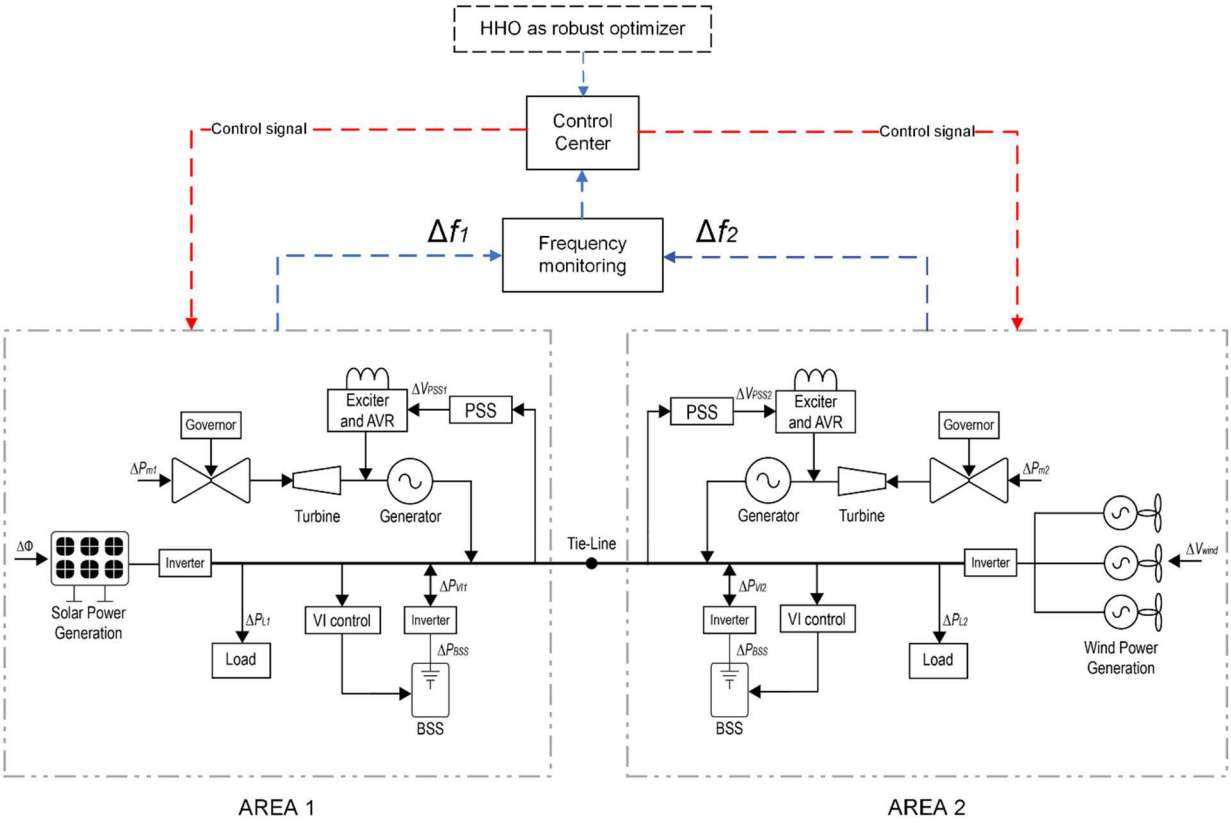

FIGURE 4. Block diagram for interconnected renewable power systems.

$$T_{3min\,a} \leq T_{3\,a} \leq T_{3,max\,a} \tag{29}$$

$$T_{4min\,a} \leq T_{4\,a} \leq T_{4,max\,a} \tag{30}$$

$$K_{VI,min\,a} \leq K_{VI\,a} \leq K_{VI,max\,a} \tag{31}$$

$$D_{VI,min\,a} \leq D_{VI\,a} \leq D_{VI,max\,a} \tag{32}$$

with $a = 1$ or 2, that represents the area of the PSS-VI has been dispatched.

Besides that, the hybrid controlling parameter for PSS-VI is constrained by the D-shape region of stability as in Figure 5. This constraint is implemented due to the CDI cannot be maximized in simple ways. The greater CDI can cause other complications and problems for the controller. Thus, this constraint is used to eliminate the candidate solution which is not fit in the D-shape region of stability, even though it has a greater CDI.

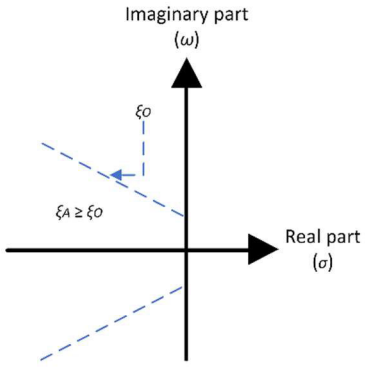

FIGURE 5. D-Shape region of stability as a constraint.

B. HHO FOR PSS-VI OPTIMIZER

Harris Hawk Optimizer (HHO) is the recent popular bio-inspired metaheuristic algorithm. The intelligence and cooperative scheme of a flock of Harris Hawk in hunting their prey inspired the researcher as in [40], to formulate the optimization method with robust exploration and exploitation processes. HHO has been proven in wide-scale implementation in various fields of research, including in power system cases [41], [42], [49]. In this paper, HHO is proposed as a robust optimizer in hybrid controlling parameters for PSS-VI illustrated on the flowchart in Figure 6. The following section describes the detailed steps in the flowchart.

1) INITIALIZATION PHASE

A flock of Harris Hawk is usually hunting in a group. The group members consist of their families or relatives. In HHO, the number of flock members is initialized as the number of population (N). The hawks spread out to observe potential prey. The initial position of hawks (X_i) is generated based on

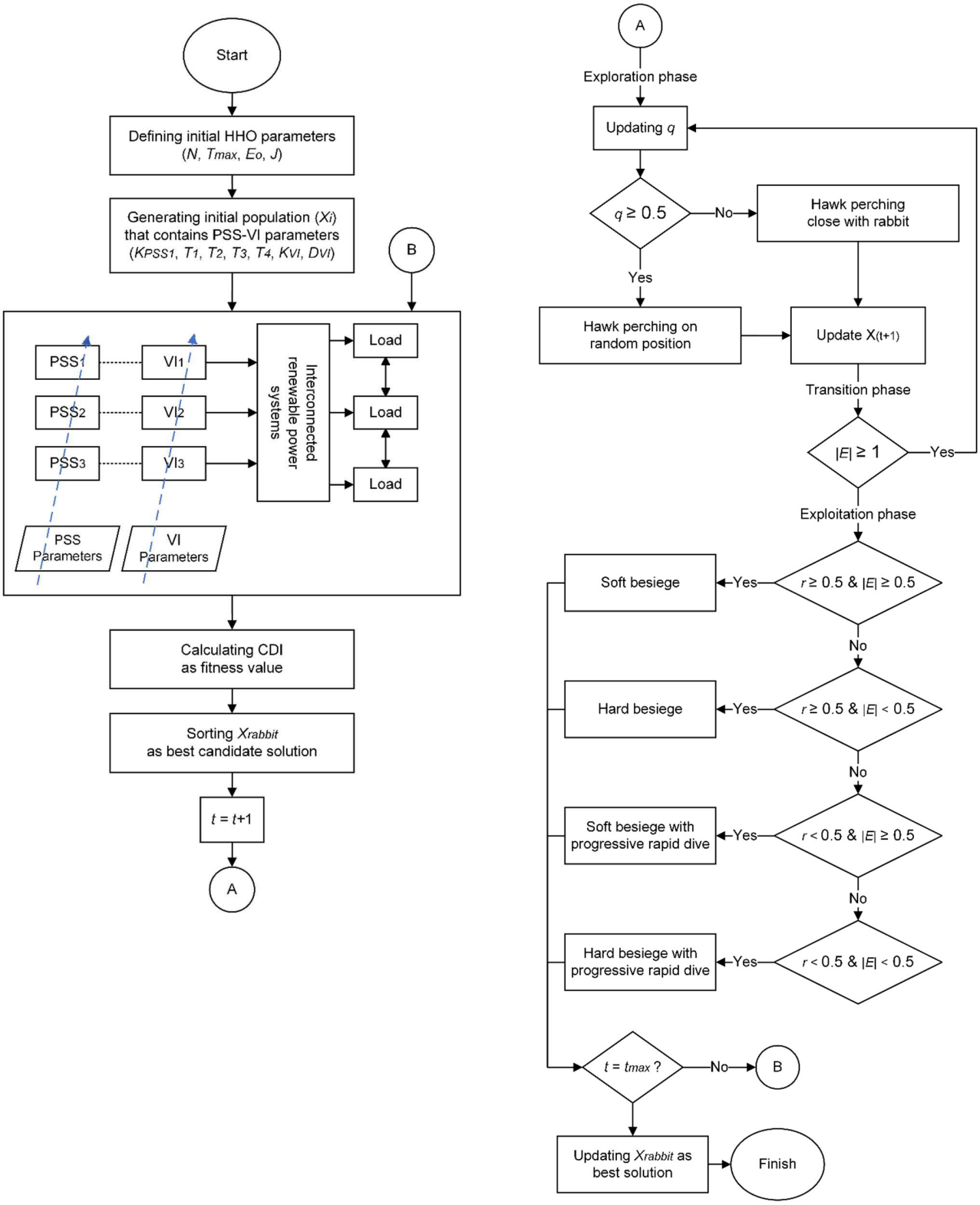

FIGURE 6. Flowchart of hybrid controlling parameter for PSS-VI.

the dimension of the optimization variable in the predetermined search space as in Equation (33).

$$X_i = [lb \leq X_i \leq ub]^D \tag{33}$$

with $i = 1, 2, \ldots, N$. lb and ub are the lower and upper bounds of search space, respectively. D is the dimension of optimization variables. In this paper, the X_i vectors are determined based on PSS-VI tunable parameters as

in Equation (26) until Equation (32). After the PSS-VI parameters are generated, the algorithm throws them into the interconnected renewable power system simulation (as illustrated with blue arrow marks). While the simulation is running, the algorithm calculates CDI in Equation (25) as a fitness value. Then, a rabbit vector (X_{rabbit}) is sorted within the search space to represent the best potential solution. A rabbit has an initial energy (E_o) and jump strength (J). The E_o is linear with the initial fitness value of X_{rabbit}. The hawks wait and observe the condition of the rabbit before the hunting begins. The rabbit condition is represented by escaping energy (E) as in Equation (34).

$$E = 2E_o(1 - \frac{t}{t_{max}}) \tag{34}$$

with t and t_{max} are the current and maximum iteration, respectively.

2) EXPLORATION PHASE

In waiting and observing their prey, the hawks are perched on high objects like trees. The hawks' position ($X\,(t+1)$) is updated along with iteration. The hawks move periodically based on Equation (35). The average position of the hawks ($X_m\,(t)$) is calculated by Equation (36), as shown at the bottom of the next page.

$$X_m\,(t) = \frac{1}{N}\sum_{i=1}^{N} X_i(t) \tag{35}$$

with $X_r(t)$ is a random movement of a hawk, $X(t)$ is current position of a hawk, $X_{rabbit}\,(t)$ is the current rabbit's location, r_1, r_2, r_3, and r_4 are random generated number between 0 to 1. The q parameter is a random value between 0 to 1 that determines the hawk's position. If $q \geq 0.5$, then the hawk perches randomly. While $q < 0.5$, the hawk perches close to the rabbit.

3) TRANSITION PHASE

A flock of hawks observes the rabbit's condition. The hawks can wait until the rabbit's energy begins to decrease or it is starting to let its guard down. In HHO, the transition phase is modeled as in Equation (37) and Equation (38).

$$E_o = \begin{cases} E_o, 0 \to 1, & \text{rabbit is still in fit condition} \\ E_o, 1 \to 0, & \text{rabbit is starting to off the guard} \end{cases} \tag{37}$$

$$phase(E) = \begin{cases} E \geq 1, & \text{still in exploration phase} \\ E < 1, & \text{start exploitation phase} \end{cases} \tag{38}$$

If E_o is still increasing from 0 to 1, then it indicates the rabbit is still in fit condition. While E_o is decreasing from 1 to 0, the rabbit is starting to off guard. Thus, if $|E| \geq 1$, then the hawks are still in the exploration phase. While $|E| < 1$, the hawks start the exploitation phase.

4) EXPLOITATION PHASE

The exploitation phase in HHO is divided into four schemes. The schemes are determined by rabbit conditions represented by the rabbit's probability of escaping (r) which has a value between 0 to 1 and $|E|$. If $r < 0.5$, then it means the rabbit tends to escape. While $r \geq 0.5$, then it means the rabbit tends to get caught. The schemes are explained in the following:

The first scheme is soft besiege ($r \geq 0.5$ and $|E| \geq 0.5$). A flock of hawks performs the soft besiege when the rabbit is still trying to escape from the hawks. The hawks surround and perform soft besiege to weaken the rabbit before launching the shock attack. The soft besiege scheme is modeled in Equation (39) until Equation (41).

$$X\,(t+1) = \Delta X(t) - E|JX_{rabbit}\,(t) - X\,(t)\,| \tag{39}$$

$$\Delta X\,(t) = X_{rabbit}\,(t) - X(t) \tag{40}$$

$$J = 2(1 - r_5) \tag{41}$$

with ΔX(t) is the average distance between the hawks and the rabbit, r_5 is a generated random number between 0 to 1.

The second scheme is hard besiege ($r \geq 0.5$ and $|E| < 0.5$). this scheme is performed by the hawks when the rabbit looks to get tired. In this scheme, the hawks surround the rabbit with heavy attacks and perform shock attacks to finish the hunting quickly. The hard besiege scheme is modeled in Equation (42).

$$X(t+1) = X_{rabbit}(t) - E|\Delta X(t)| \tag{42}$$

The third scheme is soft besiege with progressive rapid dives ($r < 0.5$ and $|E| \geq 0.5$). The rabbit still has a lot of energy to escape from the hawks. The rabbit is trying to evade the shock attack from the hawks by performing Levy Flight (LF) movements. When the hawks saw the rabbit doing LF, they tried to predict the rabbit's movement (Y) as in Equation (43).

$$Y = X_{rabbit}\,(t) - E|JX_{rabbit}\,(t) - X\,(t)\,| \tag{43}$$

If the hawks fail to predict the rabbit's movement, then the hawks execute the random dive movements to re-estimate the rabbit's pattern (Z) as in Equation (44) with LF modeled as in Equation (45) [50].

$$Z = Y + S \times LF(D) \tag{44}$$

$$LF(x) = 0.01 \times \left(\frac{u \times \sigma}{|v|^{\frac{1}{\beta}}}\right)$$

$$.\sigma = \left(\frac{\Gamma(1+\beta) \times \sin(\frac{\pi\beta}{2})}{\Gamma\left(\frac{1+\beta}{2}\right) \times \beta \times 2^{\frac{\beta-1}{2}}}\right) \tag{45}$$

with S is a random vector within $1 \times D$ size, u and v are the random generated numbers between 0 to 1, σ is the standard deviation, Γ is the gamma operator, and β is the determined constant of 1.5.

The soft besiege with progressive rapid dives scheme is modeled in Equation (46).

$$X(t+1) = \begin{cases} Y & if\ F(Y) < F(X(t)) \\ Z & if\ F(Z) < F(X(t)) \end{cases} \quad (46)$$

The fourth scheme is hard besiege with progressive rapid dives ($r < 0.5$ and $|E| < 0.5$). This scheme is performed by the hawks when the rabbit is successful in escaping. However, the hawks realize that the rabbit has become tired and let down the guard. Thus, the hawks perform progressive rapid dives to cut the distance from the rabbit. The hard besiege with progressive rapid dives scheme is similar to Equation (46). However, the Y and Z are calculated by Equation 47 and Equation (48), respectively.

$$Y = X_{rabbit}(t) - E|JX_{rabbit}(t) - X_m(t) \quad (47)$$

$$Z = Y + S \times LF(D) \quad (48)$$

The hunting processes will be completed when the hawks are successful in catching the rabbit. In HHO, the end of hunting processes is indicated with $|E|$ decreases until it approaches 0.

IV. SIMULATION AND DISCUSSION

In this section, the simulation parameters and scenarios for investigating the working behavior of interconnected renewable power systems are conducted. The discussion regarding the hybrid controlling parameter for PSS-VI is divided into several parts. The first part is related to the optimal parameter for PSS-VI by HHO compared to the other recent novel algorithms. Then, the eigenvalue analysis is also given. Besides that, the time domain simulation in renewable penetration levels is also investigated. In the rest, the proposed method in the hybrid controlling parameter for PSS-VI is validated with several performance indexes.

The simulation parameters for the interconnected renewable power system are given in Table 2. These parameters assume the simulation as follows: 1) In Area 1, the RES penetration from SPG output is less dominant, thus the base inertia properties of the system are higher; 2) In Area 2, the RES power output from WPG is more dominant, thus the base inertia properties of the system are assumed 40% lower than Area 1. From the simulation condition, the investigation cases can be arranged as in Table 3. Each case has two scenarios of RES, there are low and high levels of RES. The aim of the arranged cases is described as follows:

1) In Case 1, the change in power load occurred in Area 1. It investigates the system behavior when the transfer of energy ($\Delta P_{tie,21}$) occurs from the system with lower inertia (Area 2) to the system with higher inertia (Area 1).

TABLE 2. Parameter for interconnected renewable power systems.

Parameter	Value	
	Area 1	Area 2
Turbine time response, T_t	0.53	0.53
Governor time response, T_g	0.28	0.28
Droop constant, R_D	19.6	19.6
Bias factor, β	20.13	20.13
Control unit gain constant, K_S	0.1	0.1
WT time response, T_{WT}	-	1.4
PV time response, T_{PV}	1.9	-
Amplifier gain constant, k_A	50	50
Amplifier time constant, T_A	0.05	0.05
Exciter time response, T'_{do}	5.9	5.9
Synchronization coefficient, K_1	1.36	1.36
Electric power for flux when rotor angle is constant, K_2	0.91	0.91
Impedance factor, K_3	0.42	0.42
The demagnetizing effect, K_4	1.69	1.69
Voltage changes in the terminal when the rotor angle is changed, K_5	0.05	0.05
Voltage changes in the terminal when $E_{q'}$ is changed, K_6	0.66	0.66
Base inertia properties, H	6.5	3.9 (-40%)
Base damping properties, D	0.6	0.36 (-40%)

TABLE 3. Simulation cases for interconnected renewable power system.

Case	Scenario (RES level) 1 = low 2 = high	ΔP_{L1}	ΔP_{L2}	$\Delta\phi$	ΔV_{wind}	ΔP_{m1}	ΔP_{m2}
1	1	0.2	-	0.01	0.03	0.06	0.1
	2	0.2	-	0.06	0.1	0.01	0.03
2	1	-	0.2	0.03	0.01	0.1	0.06
	2	-	0.2	0.1	0.06	0.03	0.01
3	1	0.2	0.2	0.03	0.07	0.1	0.2
	2	0.2	0.2	0.1	0.2	0.03	0.07

2) In Case 2, the change in power load occurred in Area 2. It investigates the system behavior when the transfer of energy ($\Delta P_{tie,12}$) occurs from the system with higher inertia (Area 1) to the system with lower inertia (Area 2).
3) Case 3 investigates the system behavior when the changes in load demand have occurred in two different areas. Thus, those areas must adjust the power generation and transfer it into each area when needed.

Besides the simulation cases for interconnected renewable power systems, the other novel recent algorithms as comparisons for HHO in hybrid controlling of PSS-VI are conducted as follows:

1) Algorithm #1 (proposed optimizer): Harris Hawk Optimizer (HHO) [40].

$$X(t+1) = \begin{cases} X_r(t) - r_1|X_r(t) - 2r_2X(t)|, \&q \geq 0.5 \\ X_{rabbit}(t) - X_m(t) - r_3(lb + r_4(ub - lb)), \&q < 0.5 \end{cases} \quad (36)$$

TABLE 4. Optimal parameter for PSS-VI in interconnected renewable power system in Case 1.

Case	Scenario	Optimizer	Optimal Parameter														$f_{fitness}$
			Area 1							Area 2							
			K_{PSS}	T_1	T_2	T_3	T_4	D_{VI}	K_{VI}	K_{PSS}	T_1	T_2	T_3	T_4	D_{VI}	K_{VI}	
1	1	HHO	4.03	0.016	0.115	0.078	0.155	1.043	9.577	1.989	0.084	0.113	0.045	0.092	0.534	5.609	0.138
		EOA	0.434	0.171	0.2	0.106	0.182	0.154	6.112	0.01	0.135	0.07	0.15	0.03	0.595	1.143	0.18
		AOA	0.01	0.08	0.135	0.064	0.086	0.106	6.46	0.01	0.04	0.012	0.019	0.105	0.1	2.007	0.168
		MFO	0.01	0.182	0.143	0.073	0.179	0.294	5.826	0.066	0.091	0.021	0.061	0.072	0.1	0.371	0.142
	2	HHO	2.294	0.165	0.077	0.148	0.08	1.245	9.715	0.226	0.057	0.022	0.051	0.138	3.418	2.763	0.189
		EOA	1.607	0.197	0.167	0.081	0.137	0.102	0.577	4.344	2.296	0.109	0.16	0.117	0.108	1.406	0.223
		AOA	0.01	0.156	0.196	0.094	0.125	0.317	5.02	0.01	0.085	0.07	0.127	0.105	0.1	0.1	0.231
		MFO	0.01	0.182	0.143	0.07	0.179	0.294	5.826	0.066	0.091	0.021	0.061	0.072	0.1	0.371	0.171

TABLE 5. Optimal parameter for PSS-VI in interconnected renewable power system in Case 2.

Case	Scenario	Optimizer	Optimal Parameter														$f_{fitness}$
			Area 1							Area 2							
			K_{PSS}	T_1	T_2	T_3	T_4	D_{VI}	K_{VI}	K_{PSS}	T_1	T_2	T_3	T_4	D_{VI}	K_{VI}	
2	1	HHO	0.01	0.138	0.019	0.099	0.311	1.284	3.362	0.01	0.119	0.19	0.05	0.128	0.1	8.098	0.236
		EOA	5.48	0.012	0.097	0.143	0.113	0.42	6.194	1.031	0.107	0.171	0.092	0.01	0.266	4.34	0.299
		AOA	0.04	0.015	0.019	0.03	0.09	2	10	0.01	0.124	0.154	0.191	0.077	0.1	1.666	0.263
		MFO	0.178	0.011	0.156	0.079	0.163	0.107	10	0.014	0.049	0.01	0.057	0.112	0.257	7.92	0.294
	2	HHO	9.659	0.01	0.011	0.01	0.14	1.126	3.014	0.01	0.356	0.148	0.126	0.129	0.1	10	0.258
		EOA	8.192	0.06	0.132	0.151	0.074	0.1	10	0.01	0.152	0.161	0.036	0.01	0.296	4.254	0.26
		AOA	8.363	0.154	0.2	0.122	0.066	0.279	10	0.011	0.041	0.071	0.052	0.072	0.1	7.184	0.263
		MFO	2.562	0.094	0.151	0.035	0.053	0.646	6.564	0.02	0.075	0.021	0.054	0.13	0.124	9.397	0.34

TABLE 6. Optimal parameter for PSS-VI in interconnected renewable power system in Case 3.

Case	Scenario	Optimizer	Optimal Parameter														$f_{fitness}$
			Area 1							Area 2							
			K_{PSS}	T_1	T_2	T_3	T_4	D_{VI}	K_{VI}	K_{PSS}	T_1	T_2	T_3	T_4	D_{VI}	K_{VI}	
3	1	HHO	0.018	0.196	0.2	0.01	0.01	1.604	10	9.892	0.116	0.146	0.049	0.176	0.2	5.944	0.279
		EOA	0.013	0.075	0.151	0.138	0.093	0.673	5.881	10	0.09	0.01	0.142	0.137	0.23	10	0.244
		AOA	0.01	0.053	0.129	0.2	0.084	0.458	1.171	10	0.186	0.173	0.01	0.147	2	10	0.281
		MFO	0.096	0.175	0.015	0.04	0.125	0.329	1.507	9.721	0.078	0.033	0.087	0.104	1.621	2.257	0.298
	2	HHO	0.01	0.025	0.076	0.184	0.104	0.144	9.986	0.01	0.082	0.15	0.2	0.198	0.164	5.748	0.286
		EOA	1.766	0.151	0.179	0.2	0.2	0.44	4.052	7.548	0.114	0.022	0.045	0.162	1.567	1.589	0.307
		AOA	0.03	0.01	0.187	0.13	0.118	0.2	3.186	9.811	0.161	0.016	0.042	0.117	1.91	9.411	0.312
		MFO	0.01	0.025	0.025	0.184	0.149	0.139	9.316	0.815	0.012	0.01	0.093	0.093	0.128	1.237	0.357

2) Algorithm #2: Equilibrium Optimizer Algorithm (EOA) [51].
3) Algorithm #3: Arithmetic Optimizer Algorithm (AOA) [52].
4) Algorithm #4: Moth Flame Optimizer (MFO) [53].

A. OPTIMAL PARAMETER FOR PSS-VI

The optimal parameters for PSS-VI that have been conducted by algorithms are different in various cases and scenarios as shown in Table 4 until Table 6. It can be seen that the different cases and scenarios offer diverse optimal parameters for PSS-VI. The appropriateness of the optimal parameter can be measured by the lower fitness value. In Case 1 Scenario 1, HHO conducts the best fitness value of 0.138, which is followed by AOA, EOA, and MFO of 0.168, 0.18, and 0.142, respectively. In Case 1 Scenario 2, MFO has the best fitness value of 0.171, which is followed by HHO, EOA, and AOA of 0.189, 0.223, and 0.231, respectively. In Case 2

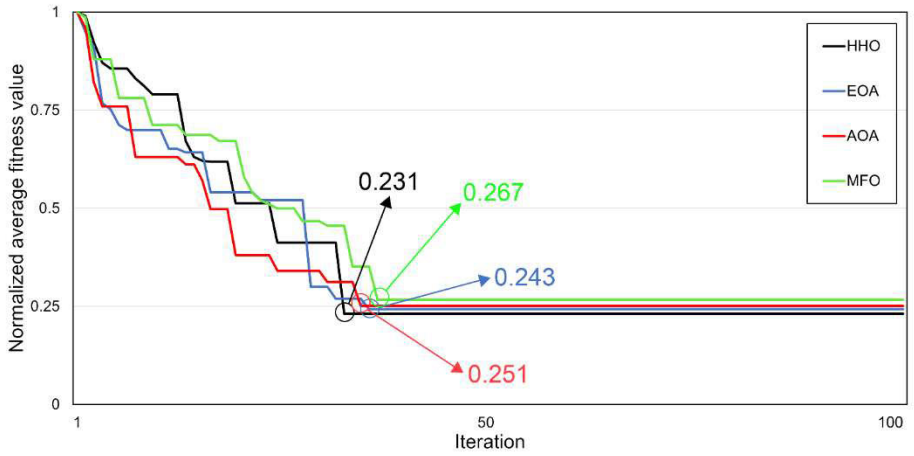

FIGURE 7. Normalized average convergence curve of the algorithm in hybrid controlling of PSS-VI.

Scenario 1, HHO gives the best fitness value of 0.236, which is followed by AOA, MFO, and EOA of 0.263, 0.294, and 0.299, respectively. In Case 2 Scenario 2, HHO brings the best fitness value of 0.258, which is followed by EOA, AOA, and MFO by 0.26, 0.263, and 0.34, respectively. In Case 3 Scenario 1, EOA delivers the best fitness value of 0.244, which is followed by HHO, AOA, and MFO of 0.279, 0.281, and 0.298, respectively. In Case 3 Scenario 2, HHO manages the best fitness value of 0.286, which is followed by EOA, AOA, and MFO of 0.307, 0.312, and 0.357, respectively.

From the results, it can be concluded that HHO is superior to the other algorithms due to HHO's success in conducting the best fitness value in 4 of 6 scenarios. Furthermore, the normalized average fitness value is presented in the convergence curve as shown in Figure 7. It can be seen that HHO has the best average value of 0.231, which is followed by EOA, AOA, and MFO of 0.243, 0.251, and 0.267, respectively. Moreover, HHO can offer its best value in the fastest iterations than the other algorithm. It supports the evidence that HHO can outperform the EOA, AOA, and MFO in hybrid controlling parameters for PSS-VI in various cases and scenarios.

B. EIGENVALUE ANALYSIS

The objective function in hybrid controlling parameters for PSS-VI is related to the CDI equation that is represented by the eigenvalue of the system as given in Table 7. The analysis can be performed by seeing the marked value by the grey highlighter. HHO gives the eigenvalue of -10.5222 ± 4.5858i (Case 1 Scenario 1), -10.4175 ± 3.7895i (Case 1 Scenario 2), -10.5222 ± 4.5858i (Case 2 Scenario 1), -10.2841 ± 4.0180i (Case 2 Scenario 2), -10.5222 ± 4.5858i (Case 3 Scenario 1), and -10.2841 ± 4.0180i (Case 3 Scenario 2). The stability of the system is dependent on the ratio of the real and imaginary parts of the eigen value. If the value becomes more negative, then it means the system has better stability. As in Figure 5, the proper method must shift the eigenvalue point to the left side. From Table 7, all of the results in the hybrid controlling parameters for PSS-VI by algorithms are successful in shifting the eigenvalue point to the left side. It indicated the proposed approach in this paper is suitable to enhance the stability based on the eigenvalue analysis. Moreover, HHO conducts the most negative value in all of the scenarios than the other algorithms. Thus, it can be concluded that HHO offers the best stability enhancement validated by eigenvalue analysis.

C. TIME DOMAIN SIMULATION

An in-depth analysis regarding the result of hybrid controlling parameters for PSS-VI is conducted using time domain simulation. This section investigates the frequency responses in Area 1 and Area 2 of interconnected renewable power systems. Besides that, the power change characteristic through tie-line ($\Delta P_{tie,12}$ or $\Delta P_{tie,21}$) is also presented. In this paper, the dynamic stability improvement indicated by RoCoF reduction can be clearly seen using time domain simulation. Moreover, the detailed responses of the interconnected renewable are also given. As explained in Table 3, the Case in this paper is focused on investigating the system behavior in different ΔP_L, $\Delta\phi$, and ΔV_{wind} as the input for various small-signal disturbances occurred in the interconnected renewable power systems. Meanwhile, the Scenario is focused on the RES-level conditions. Scenario 1 simulates the low-RES level condition, while Scenario 2 simulates the high-RES level condition. The detailed investigation is given in the following.

1) CASE 1

In Case 1, $\Delta P_L = 0.2$ in Area 1. The ΔP_{SPG} and ΔP_{WPG} are linearly affected by $\Delta\phi$ and ΔV_{wind}, respectively. In this case, the output power from Area 2 is higher than Area 1 to simulate the condition when the transfer of energy occurs from the system with lower inertia (Area 2) to the system with higher inertia (Area 1). The Δf_1 and Δf_2 responses of hybrid controlling for PSS-VI in low-RES level conditions are shown by Figure 8 and Figure 9. Besides that, the $\Delta P_{tie2,1}$ response in low-RES level conditions is given by Figure 10. Moreover, a detailed response in statistics is summarized by Table 8. In this paper, the stability enhancement aims to

TABLE 7. Investigated eigenvalue for interconnected renewable power systems with hybrid controlling of PSS-VI.

Optimizer	Eigenvalue					
	Case 1		Case 2		Case 3	
	Scenario 1	Scenario 2	Scenario 1	Scenario 2	Scenario 1	Scenario 2
HHO	-10.5222 ± 4.5858i -10.8511 ± 4.1862i -5.5259 ± 1.4774i -4.4683 ± 1.3106i -0.4526 ± 2.6649i -0.4753 ± 2.4785i	-10.4175 ± 3.7895i -10.2841 ± 4.0180i -6.5446 ± 0.3387i -0.8919 ± 2.6352i -0.6124 ± 2.1917i -0.1031 ± 0.2018i	-10.5222 ± 4.5858i -10.8511 ± 4.1862i -5.5259 ± 1.4774i -4.4683 ± 1.3106i -0.4526 ± 2.6649i -0.4753 ± 2.4785i -0.1146 ± 0.2080i	-10.2841 ± 4.0180i -9.3133 ± 5.7528i -6.5446 ± 0.3387i -0.8912 ± 2.6362i -0.5195 ± 2.1626i -0.1052 ± 0.1997i	-10.5222 ± 4.5858i -10.8711 ± 4.1943i -5.5265 ± 1.5333i -4.4683 ± 1.3106i -0.5447 ± 2.7066i -0.4738 ± 2.4682i -0.1110 ± 0.2067i	-10.2841 ± 4.0180i -9.3133 ± 5.7528i -6.5446 ± 0.3387i -0.8912 ± 2.6362i -0.5195 ± 2.1626i -0.1052 ± 0.1997i
EOA	-10.2226 ± 3.9991i -10.2266 ± 4.0542i -4.8833 ± 0.3542i -0.3711 ± 2.4803i -0.2554 ± 2.1134i -0.1348 ± 0.2019i	-10.0869 ± 3.3189i -9.2902 ± 5.7904i -6.3104 ± 1.1244i -5.6361 ± 1.0467i -0.4072 ± 2.6340i -0.4185 ± 2.2131i -0.1243 ± 0.2046i	-10.2226 ± 3.9991i -10.2266 ± 4.0542i -4.8833 ± 0.3542i -0.3711 ± 2.4803i -0.2554 ± 2.1134i -0.1348 ± 0.2019i	-10.0869 ± 3.3189i -10.4175 ± 3.7895i -5.6361 ± 1.0467i -6.3104 ± 1.1244i -0.4072 ± 2.6340i -0.4185 ± 2.2131i -0.1243 ± 0.2046i	-10.2226 ± 3.9991i -10.2244 ± 4.0512i -4.8833 ± 0.3542i -0.1890 ± 2.3946i -0.2570 ± 2.1253i -0.1461 ± 0.2036i	-10.0869 ± 3.3189i -10.4175 ± 3.7895i -5.6361 ± 1.0467i -6.3104 ± 1.1244i -0.4072 ± 2.6340i -0.4185 ± 2.2131i -0.1243 ± 0.2046i
AOA	-10.2121 ± 4.0328i -10.2228 ± 4.0414i -0.1698 ± 2.3883i -0.2235 ± 2.0898i -0.1486 ± 0.2020i	-10.2116 ± 4.0429i -10.2108 ± 4.0322i -0.1686 ± 2.3868i -0.2553 ± 2.1038i -0.1478 ± 0.2032i	-10.2121 ± 4.0328i -10.2228 ± 4.0414i -0.1698 ± 2.3883i -0.2235 ± 2.0898i -0.1486 ± 0.2020i	-10.2116 ± 4.0429i -10.2108 ± 4.0322i -0.1686 ± 2.3868i -0.2553 ± 2.1038i -0.1478 ± 0.2032i	-10.2121 ± 4.0328i -10.2228 ± 4.0414i -0.1698 ± 2.3883i -0.2235 ± 2.0898i -0.1486 ± 0.2020i	-10.2116 ± 4.0429i -10.2108 ± 4.0322i -0.1686 ± 2.3868i -0.2553 ± 2.1038i -0.1478 ± 0.2032i
MFO	-10.2121 ± 4.0328i -10.2228 ± 4.0414i -0.1698 ± 2.3883i -0.2235 ± 2.0898i	-10.2236 ± 4.0188i -10.2074 ± 4.0522i -4.9087 ± 0.3807i -0.1663 ± 2.3873i -0.3730 ± 2.1675i -0.1439 ± 0.2073i	-10.2118 ± 4.0325i -10.2008 ± 4.0429i -0.1759 ± 2.3918i -0.2517 ± 2.1019i -0.1474 ± 0.2030i	-10.2074 ± 4.0522i -10.2236 ± 4.0188i -4.9087 ± 0.3807i -0.1663 ± 2.3873i -0.3730 ± 2.1675i -0.1439 ± 0.2073i	-10.2118 ± 4.0325i -10.2008 ± 4.0429i -0.1759 ± 2.3918i -0.2517 ± 2.1019i -0.1474 ± 0.2030i	-10.2074 ± 4.0522i -10.2236 ± 4.0188i -0.1663 ± 2.3873i -0.3730 ± 2.1675i -0.1439 ± 0.2073i

TABLE 8. Detailed response in Case 1 Scenario 1 of hybrid controlling for PSS-VI.

Response	Parameter	PSS-VI Optimizer			
		HHO	EOA	AOA	MFO
Δf_1	RoCoF (p.u, %)	-8.89 x 10^{-3}, -0.88%	-1.01 x 10^{-2}, -1.01%	-1.02 x 10^{-2}, -1.02%	-1.04 x 10^{-2}, -1.04%
	Overshoot (p.u.)	+1.24 x 10^{-3}	+2.74 x 10^{-3}	+3.28 x 10^{-3}	+2.87 x 10^{-3}
	Settling time (s)	16.96	14.59	14.91	14.92
Δf_2	RoCoF (p.u, %)	+1.96 x 10^{-3}, +0.19%	+2.35 x 10^{-3}, +0.23%	+2.87 x 10^{-3}, +0.28%	+2.55 x 10^{-3}, +0.25%
	Undershoot (p.u.)	-2.24 x 10^{-3}	-3.03 x 10^{-3}	-2.35 x 10^{-3}	-2.29 x 10^{-3}
	Settling time (s)	21.07	19.28	19.46	19.66
$\Delta P_{tie,21}$	RoCoF (p.u, %)	-4.87 x 10^{-2}, -4.87%	-5.45 x 10^{-2}, -5.45%	-5.89 x 10^{-2}, -5.89%	-5.67 x 10^{-2}, -5.67%
	Overshoot (p.u.)	+7.9 x 10^{-3}	+7.1 x 10^{-3}	+4.64 x 10^{-3}	+4.55 x 10^{-3}
	Settling time (s)	26.19	22.9	14.93	15.11

suppress the RoCoF when the disturbance occurs. Based on Figure 8, the hybrid controlling for PSS-VI by HHO conducts the smallest RoCoF in Δf_1 of −0.88% which is followed by EOA, AOA, and MFO of −1.01%, −1.02%, and −1.04%, respectively.

In Figure 9, HHO has also conducted the smallest RoCoF in Δf_2 of +0.19%, which is followed by EOA, MFO, and AOA of +0.23%, +0.25%, and +0.28%, respectively. Figure 10 shows the negative RoCoF that indicates a power transfer from Area 2 into Area 1. It can be seen that HHO also gives the lowest RoCoF in $\Delta P_{tie,21}$ of −4.87%, which is followed by EOA, MFO, and AOA of −5.45%, −5.67%, and −5.89%, respectively.

In Scenario 2 (high-RES level condition), the Δf_1, Δf_2, and $\Delta P_{tie,21}$ are given in Figure 11, Figure 12, and Figure 13, respectively. A detailed response is also presented in Table 9. HHO is successful in giving the smallest RoCoF in Δf_1 of −0.77%, which is followed by MFO, EOA, and AOA of −0.93%, −1.01%, and −1.07%, respectively.

In Δf_2, HHO has also offered the smallest RoCoF of +4.19%, which is followed by EOA, AOA, and MFO of +4.62%, +5.76%, and 6.04%, respectively. In this scenario,

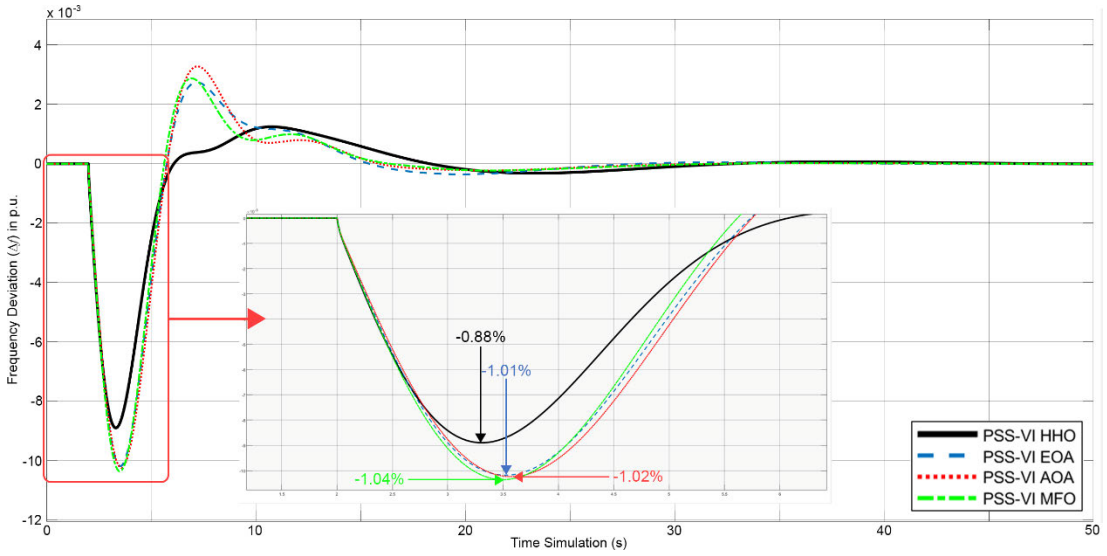

FIGURE 8. Δf_1 response in Case 1 Scenario 1 of hybrid controlling for PSS-VI.

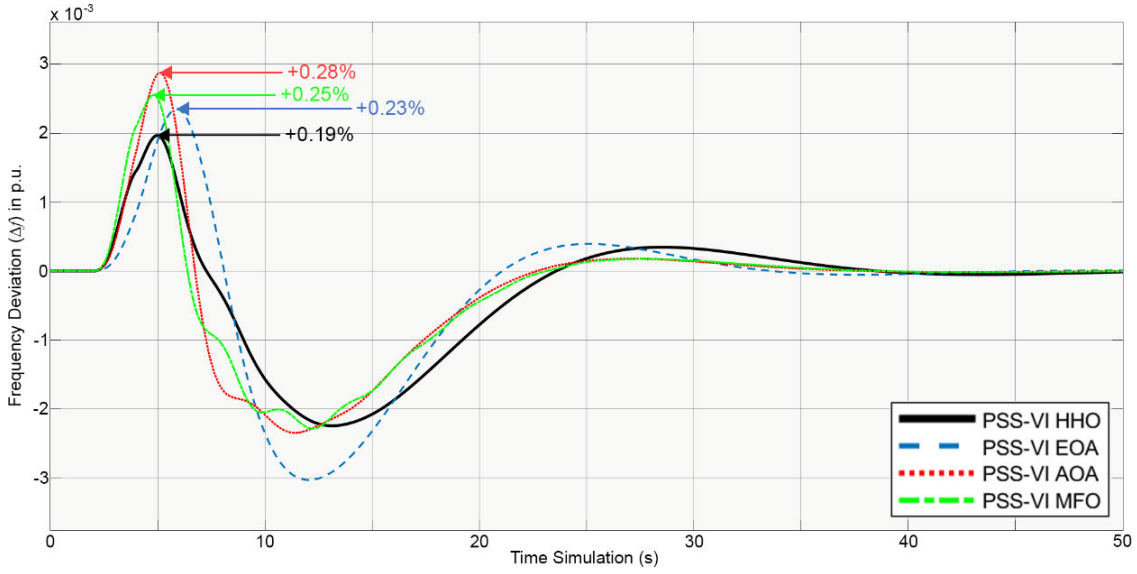

FIGURE 9. Δf_2 response in Case 1 Scenario 1 of hybrid controlling for PSS-VI.

the smallest RoCoF in $\Delta P_{tie,21}$ is obtained by EOA of -5.43%, which is followed by HHO, AOA, and MFO of -5.99%, -6.12%, and -6.26%, respectively.

The time domain simulation in Case 1 has concluded that the hybrid controlling for PSS-VI by HHO offers the overall best RoCoF reduction in the system than the other algorithms. However, the overshoot or undershoot and settling time sometimes become a bit higher than the others. This is the compensation that must be paid to get a smoother oscillation and transition in responses.

2) CASE 2

In Case 2, $\Delta P_L = 0.2$ in Area 2. The output power from Area 1 is higher than Area 2 to simulate the transfer of energy ($\Delta P_{tie1,2}$) that occurs from the system with higher inertia (Area 1) to the system with lower inertia (Area 2). Figure 14, Figure 15, and Figure 16 present the Δf_1, Δf_2, and $\Delta P_{tie,21}$ in Scenario 1, respectively. The detailed statistics are presented in Table 10. It can be seen that HHO offers the best RoCoF reduction in Δf_1 of -0.18%, which is followed by EOA of -0.29%, AOA and MFO give similar results of -2.63%. HHO has conducted the smallest RoCoF in Δf_2 of -1.01%, which is followed by EOA, AOA, and MFO of -1.03%, -1.46%, and -1.53%, respectively. Then, $\Delta P_{tie,21}$ in the positive RoCoF indicates the power transfer from Area 1 into Area 2 can be seen in Figure 16. HHO has the lowest RoCoF in $\Delta P_{tie,21}$ of $+5.34\%$, which is followed by MFO, AOA, and EOA of $+5.24\%$, $+5.37\%$, and $+5.62\%$.

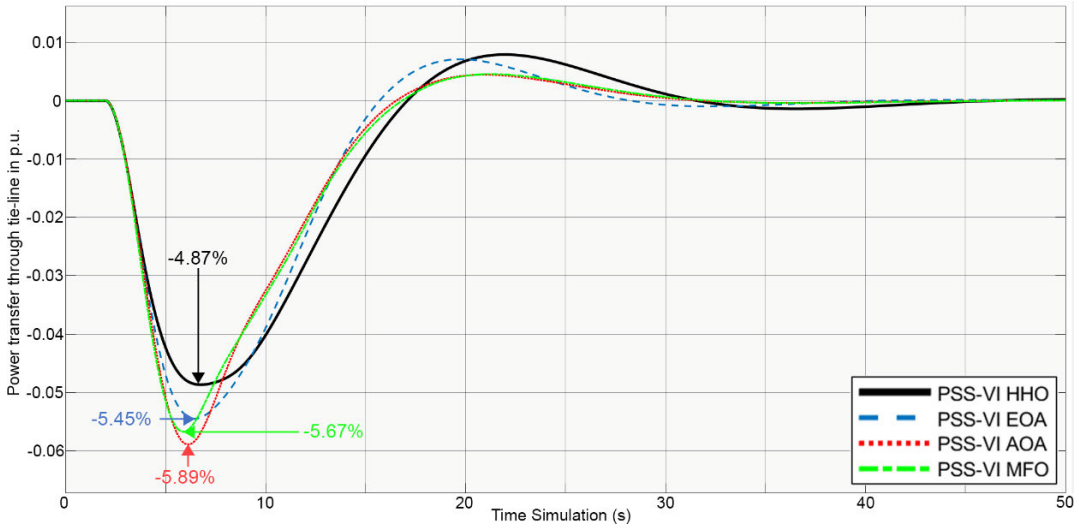

FIGURE 10. $\Delta P_{tie,21}$ response in Case 1 Scenario 1 of hybrid controlling for PSS-VI.

TABLE 9. Detailed response in Case 1 Scenario 2 of hybrid controlling for PSS-VI.

Response	Parameter	PSS-VI Optimizer			
		HHO	EOA	AOA	MFO
Δf_1	RoCoF (p.u, %)	-7.75 x 10^{-3}, -0.77%	-1.01 x 10^{-2}, -1.01%	-1.07 x 10^{-2}, -1.07%	-9.38 x 10^{-3}, -0.93%
	Overshoot (p.u.)	+3.31 x 10^{-3}	+2.9 x 10^{-3}	+4.77 x 10^{-3}	+4 x 10^{-3}
	Settling time (s)	16.12	15.71	14.47	15.03
Δf_2	RoCoF (p.u, %)	+4.19 x 10^{-3}, +4.19%	+4.62 x 10^{-3}, +4.62%	+5.76 x 10^{-3}, +5.76%	+6.04 x 10^{-3}, +6.04%
	Undershoot (p.u.)	-2.26 x 10^{-3}	-2.1 x 10^{-3}	-2.55 x 10^{-3}	-2.63 x 10^{-3}
	Settling time (s)	21.62	20.93	20.44	20.3
$\Delta P_{tie,21}$	RoCoF (p.u, %)	-5.99 x 10^{-2}, -5.99%	-5.43 x 10^{-2}, -5.43%	-6.12 x 10^{-2}, -6.12%	-6.26 x 10^{-2}, -6.26%
	Overshoot (p.u.)	+9.86 x 10^{-3}	7.2 x 10^{-3}	4.84 x 10^{-3}	5.52 x 10^{-3}
	Settling time (s)	26.92	25.63	22.93	21.05

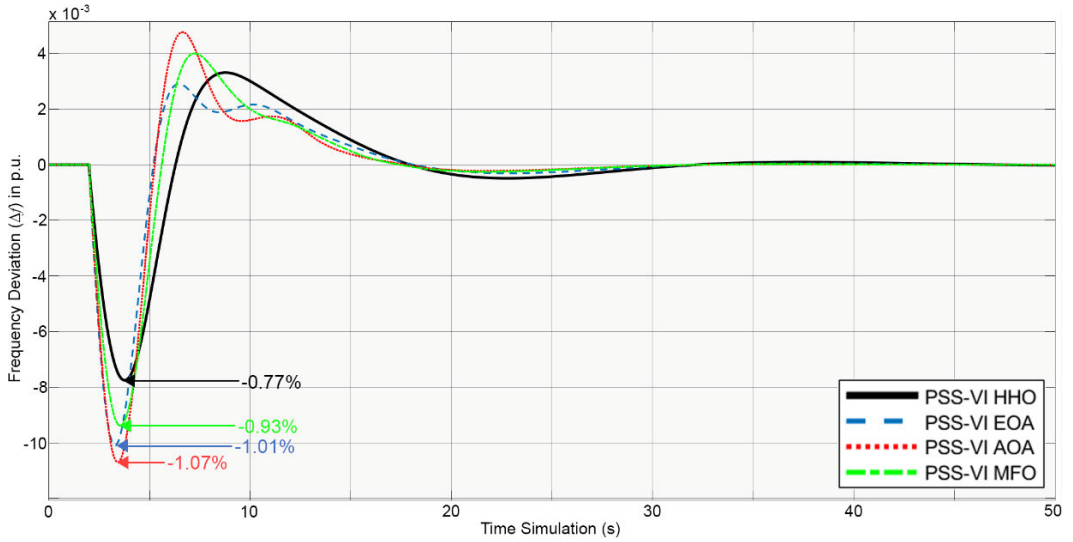

FIGURE 11. Δf_1 response in Case 1 Scenario 2 of hybrid controlling for PSS-VI.

In Scenario 2, the Δf_1, Δf_2, and $\Delta P_{tie,21}$ are presented in Figure 17, Figure 18, and Figure 19, respectively. Moreover, the detailed response is shown in Table 11. It can be seen that the HHO has also superior results than the other algorithms.

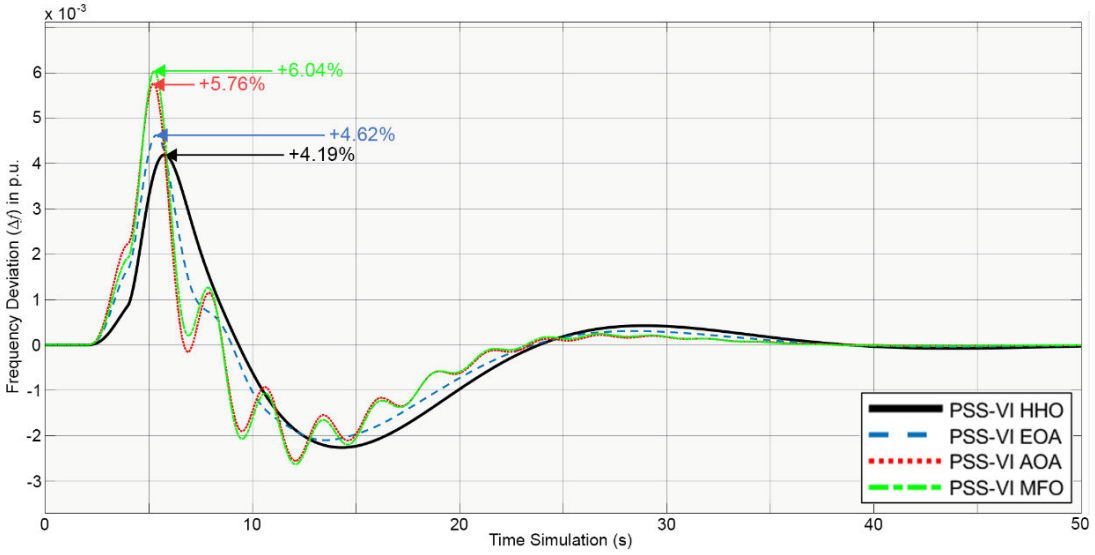

FIGURE 12. Δf_2 response in Case 1 Scenario 2 of hybrid controlling for PSS-VI.

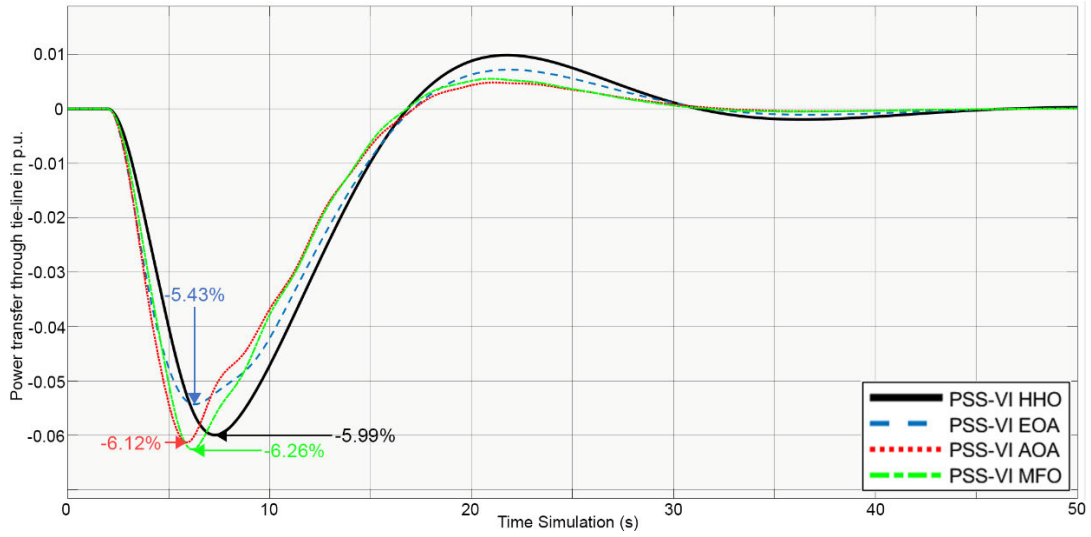

FIGURE 13. $\Delta P_{tie,21}$ response in Case 1 Scenario 2 of hybrid controlling for PSS-VI.

TABLE 10. Detailed response in Case 2 Scenario 1 of hybrid controlling for PSS-VI.

Response	Parameter	PSS-VI Optimizer			
		HHO	EOA	AOA	MFO
Δf_1	RoCoF (p.u, %)	-1.8 x 10^{-3}, -0.18%	-2.92 x 10^{-3}, -0.29%	-2.63 x 10^{-3}, -0.26%	-2.63 x 10^{-3}, -0.26%
	Overshoot (p.u.)	+4.67 x 10^{-4}	+3.89 x 10^{-4}	+2.07 x 10^{-4}	+2.04 x 10^{-4}
	Settling time (s)	14.91	11.13	13.27	13.07
Δf_2	RoCoF (p.u, %)	-1.01 x 10^{-2}, -1.01%	-1.03 x 10^{-2}, -1.03%	-1.46 x 10^{-2}, -1.46%	-1.53 x 10^{-2}, -1.53%
	Overshoot (p.u.)	+2.7 x 10^{-3}	+3.47 x 10^{-3}	+2.39 x 10^{-3}	+2.29 x 10^{-3}
	Settling time (s)	20.55	17.22	19.29	19.49
$\Delta P_{tie,12}$	RoCoF (p.u, %)	+5.34 x 10^{-2}, +5.34%	+5.62 x 10^{-2}, +5.62%	+5.37 x 10^{-2}, +5.37%	+5.24 x 10^{-2}, +5.24%
	Undershoot (p.u.)	-9.82 x 10^{-3}	-7.37 x 10^{-3}	-4.05 x 10^{-3}	-4.15 x 10^{-3}
	Settling time (s)	25.27	20.76	15.01	15.15

In Δf_1, HHO can give the lowest RoCoF of -0.11%, which is followed by EOA, MFO, and AOA of -0.15%, -0.21%, and -0.22%, respectively. In Δf_2, HHO also offers the lowest RoCoF of -0.98%, which is followed by EOA, AOA,

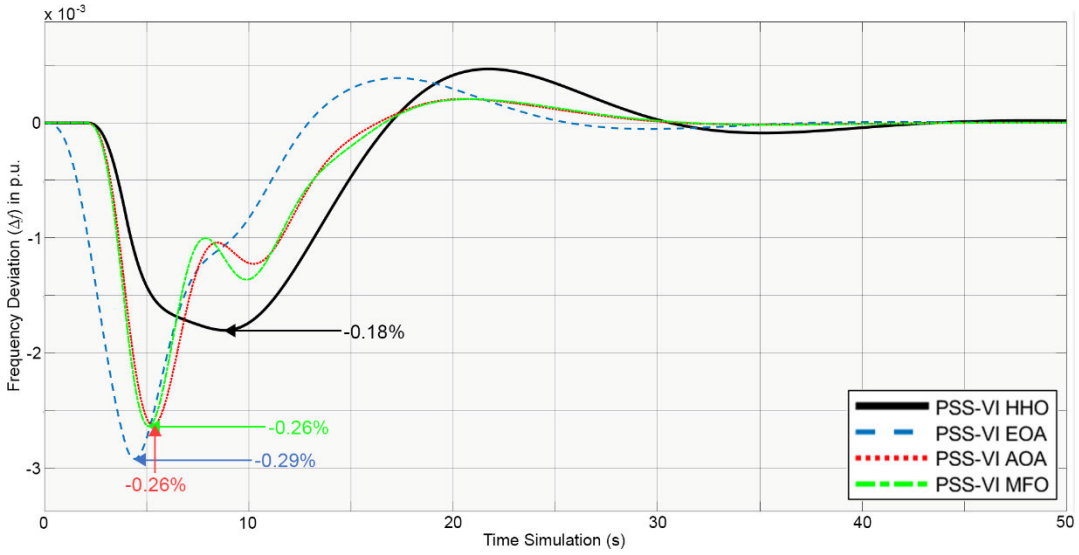

FIGURE 14. Δf_1 response in Case 2 Scenario 1 of hybrid controlling for PSS-VI.

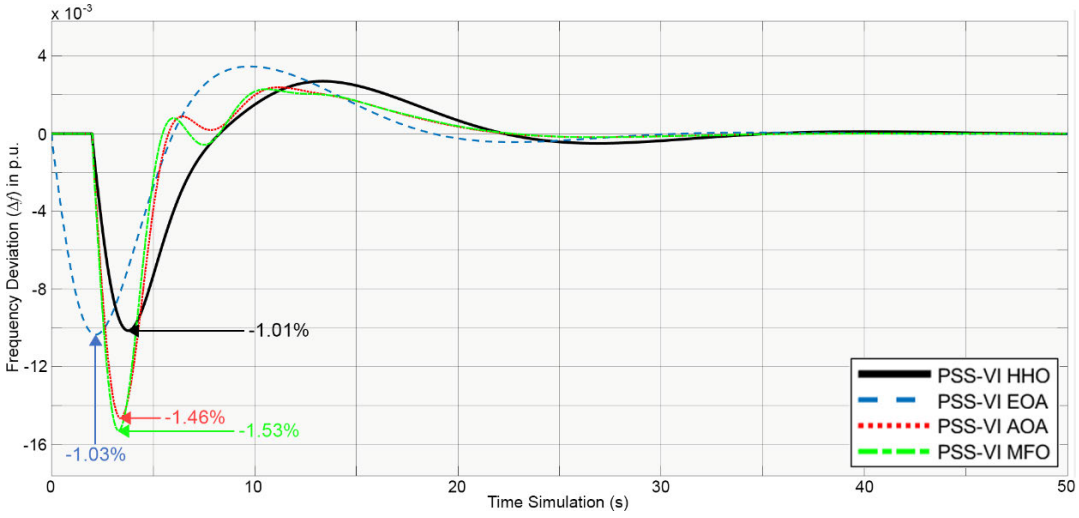

FIGURE 15. Δf_2 response in Case 2 Scenario 1 of hybrid controlling for PSS-VI.

TABLE 11. Detailed response in Case 2 Scenario 2 of hybrid controlling for PSS-VI.

Response	Parameter	PSS-VI Optimizer			
		HHO	EOA	AOA	MFO
Δf_1	RoCoF (p.u, %)	-1.12 x 10^{-3}, -0.11%	-1.53 x 10^{-3}, -0.15%	-2.25 x 10^{-3}, -0.22%	-2.13 x 10^{-3}, -0.21%
	Overshoot (p.u.)	+5.89 x 10^{-4}	+6.8 x 10^{-4}	+1.39 x 10^{-3}	+1.14 x 10^{-3}
	Settling time (s)	15.09	13.65	11.6	12.8
Δf_2	RoCoF (p.u, %)	-9.85 x 10^{-3}, -0.98%	-1.24 x 10^{-2}, -1.24%	-1.58 x 10^{-2}, -1.58%	-1.74 x 10^{-2}, -1.74%
	Overshoot (p.u.)	+2.63 x 10^{-3}	+2.59 x 10^{-3}	+3.09 x 10^{-3}	+3.31 x 10^{-3}
	Settling time (s)	21.22	22.5	20.04	20.63
$\Delta P_{tie,21}$	RoCoF (p.u, %)	+4.98 x 10^{-2}, +4.98%	+4.78 x 10^{-2}, +4.78%	+5.14 x 10^{-2}, +5.14%	+5.06 x 10^{-2}, +5.06%
	Undershoot (p.u.)	-9.4 x 10^{-3}	-6.47 x 10^{-3}	-4.09 x 10^{-3}	-4.21 x 10^{-3}
	Settling time (s)	27.52	24.94	15.93	16.07

and MFO of −1.24%, −1.58%, and −1.74%, respectively. $\Delta P_{tie,12}$ in this scenario has also produced positive RoCoF due to power transfer from Area 1 into Area 2. In this scenario, EOA gives the lowest reduction in $\Delta P_{tie,12}$ of +4.78%,

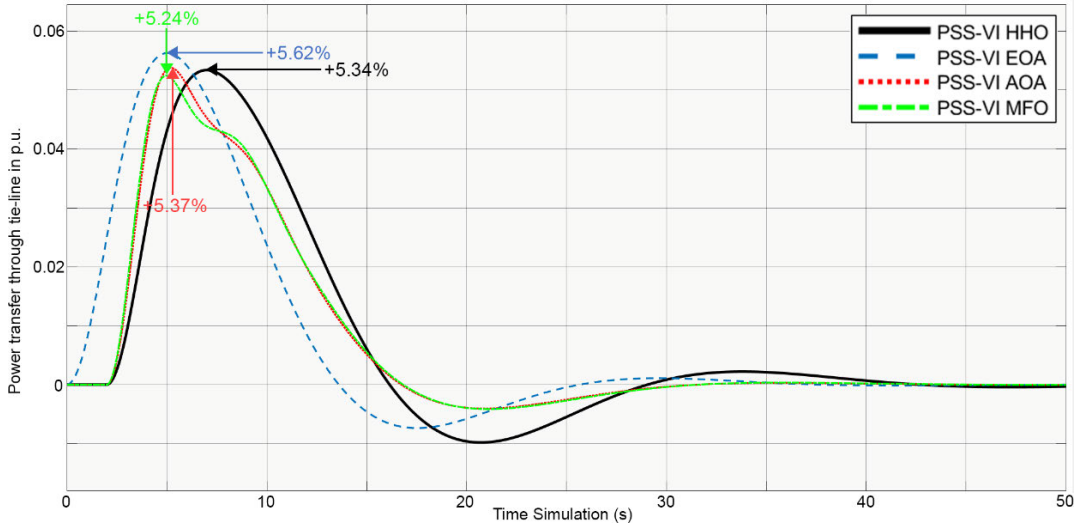

FIGURE 16. $\Delta P_{tie,12}$ response in Case 2 Scenario 1 of hybrid controlling for PSS-VI.

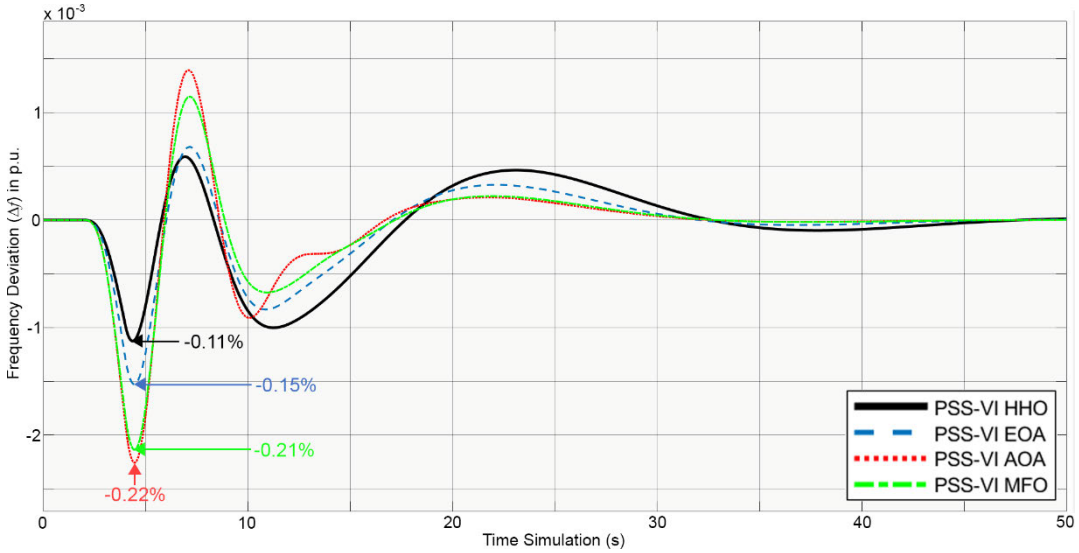

FIGURE 17. Δf_1 response in Case 2 Scenario 2 of hybrid controlling for PSS-VI.

TABLE 12. Detailed response in Case 3 Scenario 1 of hybrid controlling for PSS-VI.

Response	Parameter	PSS-VI Optimizer			
		HHO	EOA	AOA	MFO
Δf_1	RoCoF (p.u, %)	-8.76 x 10^{-3}, -0.87%	-1.17 x 10^{-2}, -1.17%	-1.13 x 10^{-2}, -1.13%	-1.14 x 10^{-2}, -1.14%
	Overshoot (p.u.)	+4.14 x 10^{-4}	+6.19 x 10^{-4}	+2.01 x 10^{-3}	+1.74 x 10^{-3}
	Settling time (s)	8.59	11.67	9.31	8.67
Δf_2	RoCoF (p.u, %)	-9.59 x 10^{-3}, -0.95%	-1.12 x 10^{-2}, -1.12%	-1.4 x 10^{-2}, -1.4%	-1.47 x 10^{-2}, -1.47%
	Overshoot (p.u.)	+1.12 x 10^{-3}	+2.52 x 10^{-3}	+4.42 x 10^{-3}	+4.53 x 10^{-3}
	Settling time (s)	18.73	17.7	15.23	14.33
$\Delta P_{tie,21}$	RoCoF (p.u, %)	+3.11 x 10^{-3}, +0.31%	+7.77 x 10^{-3}, +0.77%	+1.03 x 10^{-2}, +1.03%	+1.12 x 10^{-2}, +1.12%
	Undershoot (p.u.)	-1.16 x 10^{-2}	-1.09 x 10^{-2}	-1.75 x 10^{-2}	-1.67 x 10^{-2}
	Settling time (s)	31.32	31.57	27.1	27.82

which is followed by HHO, MFO, and AOA of +4.98%, +5.06%, and +5.14%, respectively.

Case 2 has a linear conclusion with Case 1. First, the hybrid controlling for PSS-VI by HHO is superior to

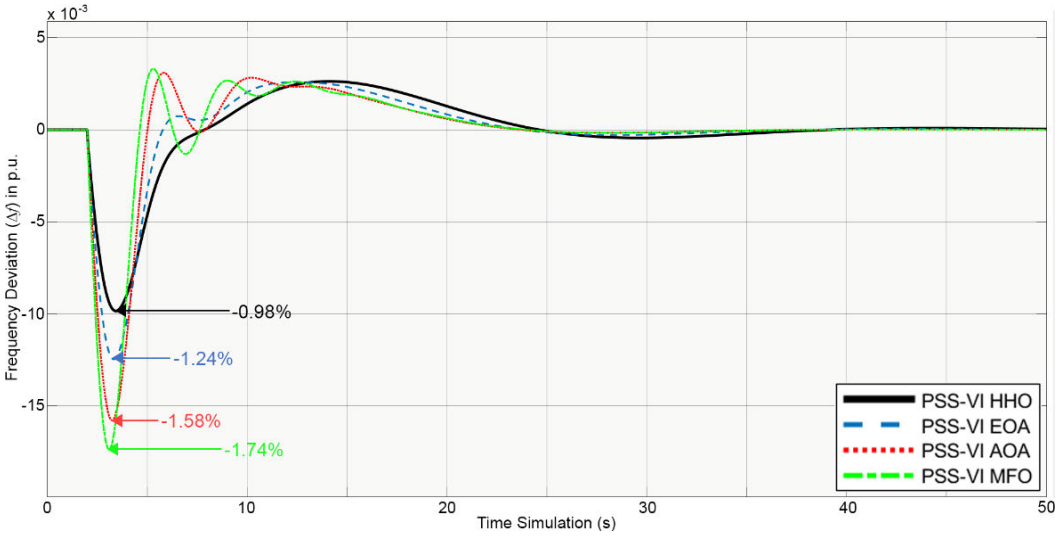

FIGURE 18. Δf_2 response in Case 2 Scenario 2 of hybrid controlling for PSS-VI.

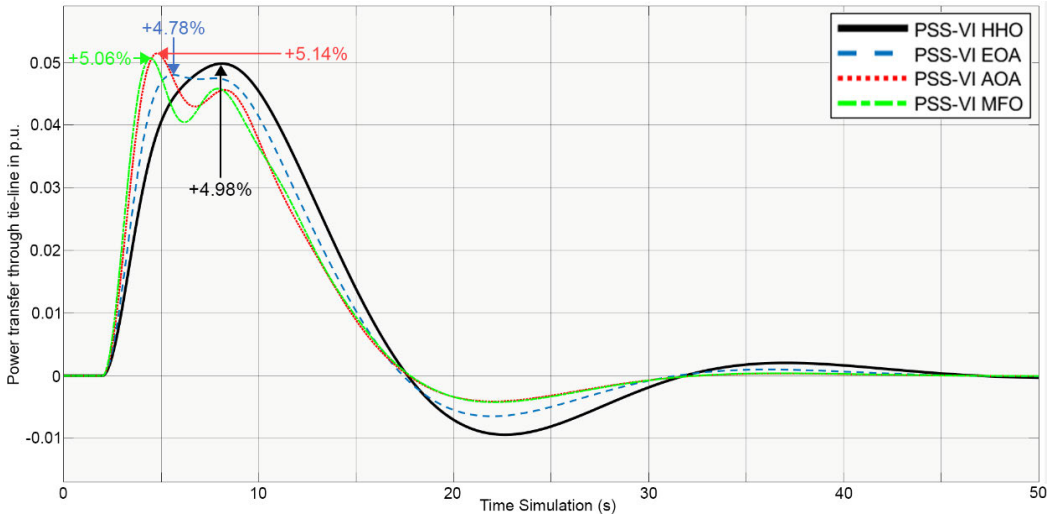

FIGURE 19. $\Delta P_{tie,12}$ response in Case 2 Scenario 2 of hybrid controlling for PSS-VI.

TABLE 13. Detailed response in Case 3 Scenario 2 of hybrid controlling for PSS-VI.

Response	Parameter	PSS-VI Optimizer			
		HHO	EOA	AOA	MFO
Δf_1	RoCoF (p.u, %)	-9.48 x 10^{-3}, -0.94%	-1.01 x 10^{-2}, -1.01%	-1.18 x 10^{-2}, -1.18%	-1.07 x 10^{-2}, -1.07%
	Overshoot (p.u.)	+2.27 x 10^{-3}	+2.92 x 10^{-3}	+4.64 x 10^{-3}	+4.05 x 10^{-3}
	Settling time (s)	16.97	16.2	14.77	15.58
Δf_2	RoCoF (p.u, %)	-9.41 x 10^{-3}, -0.94%	-1.19 x 10^{-2}, -1.19%	-1.51 x 10^{-2}, -1.51%	-1.69 x 10^{-2}, -1.69%
	Overshoot (p.u.)	+4.4 x 10^{-3}	+6.91 x 10^{-3}	+1.04 x 10^{-2}	+1.07 x 10^{-2}
	Settling time (s)	21.52	20.44	19.27	19.16
$\Delta P_{tie,21}$	RoCoF (p.u, %)	+3.71 x 10^{-3}, +0.37%	+7.19 x 10^{-3}, +0.79%	+1.09 x 10^{-2}, +1.09%	+1.89 x 10^{-2}, +1.89%
	Undershoot (p.u.)	-2.14 x 10^{-2}	-2.54 x 10^{-2}	-2.89 x 10^{-2}	-3.29 x 10^{-2}
	Settling time (s)	30.09	30.51	31.16	32.43

conducting the lowest RoCoF in the system than the others. However, it must be compensated by a bit higher overshoot or undershoot and slower settling time. Overall, the hybrid controlling parameters for PSS-VI in Case 2 have concluded that HHO offers a smoother response and transition.

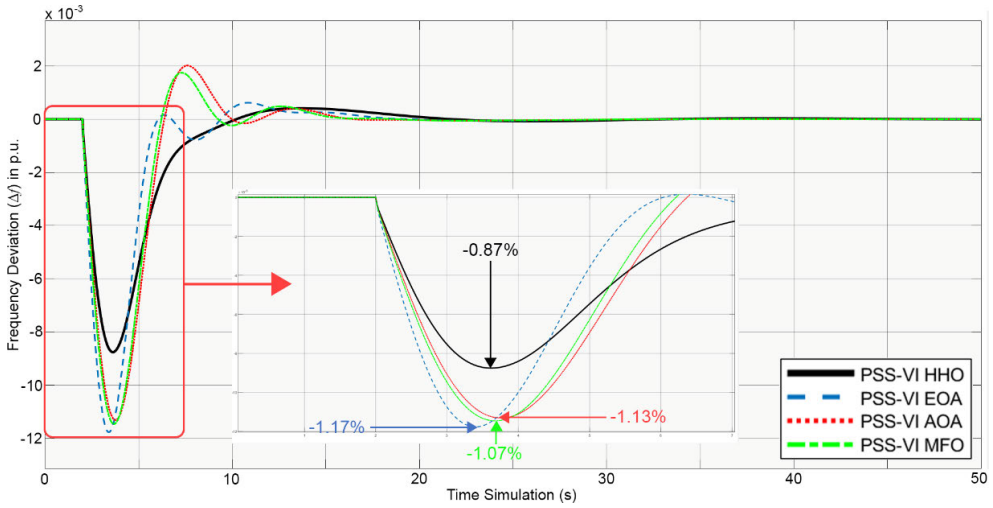

FIGURE 20. Δf_1 response in Case 3 Scenario 1 of hybrid controlling for PSS-VI.

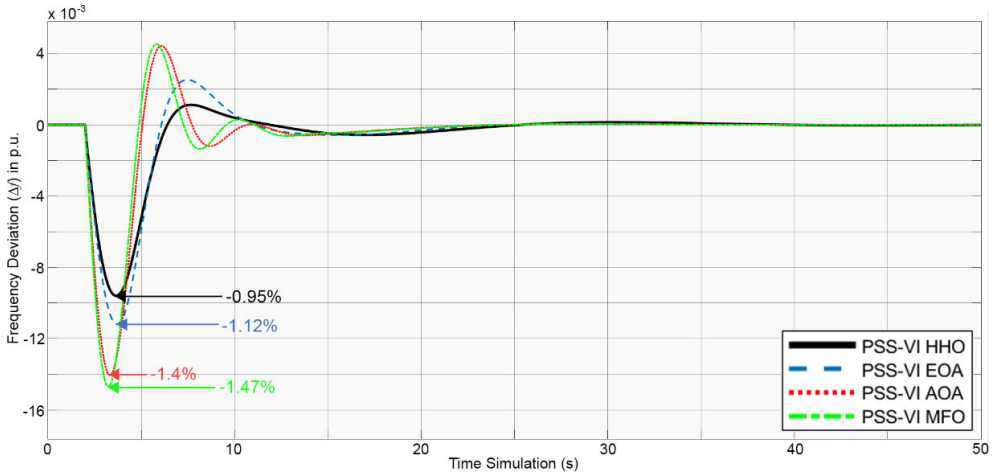

FIGURE 21. Δf_2 response in Case 3 Scenario 1 of hybrid controlling for PSS-VI.

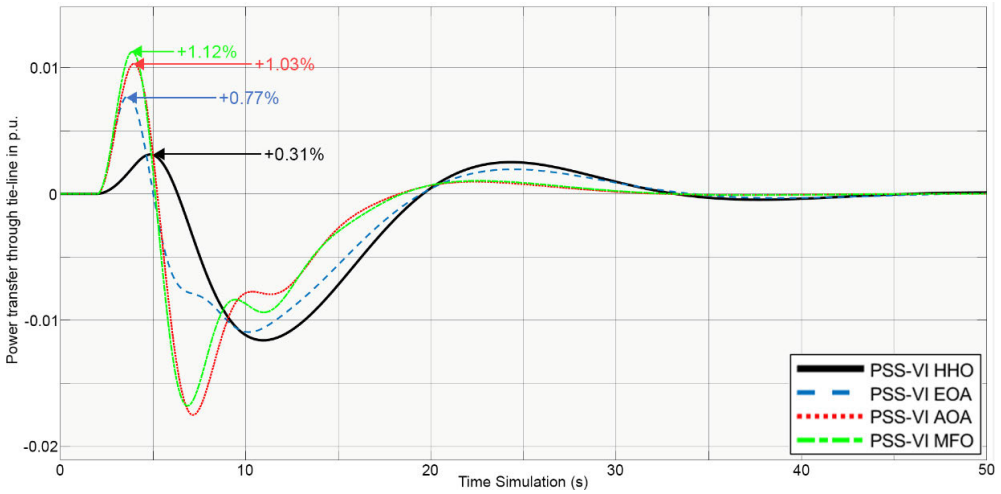

FIGURE 22. $\Delta P_{tie,12}$ response in Case 3 Scenario 1 of hybrid controlling for PSS-VI.

3) CASE 3

In Case 3, the simulation is conducted to investigate the more complex working conditions in interconnected renewable power systems. It assumed that $\Delta P_L = 0.2$ in Area 1 and Area 2, simultaneously. In this case, the power output in Area 2 is higher than in Area 1 in both Scenario 1

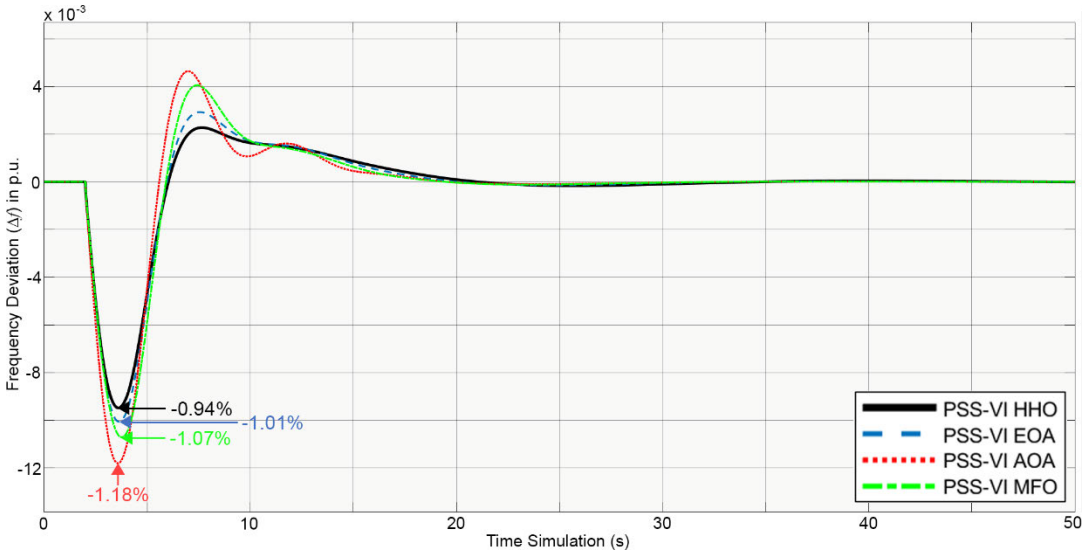

FIGURE 23. Δf_1 response in Case 3 Scenario 2 of hybrid controlling for PSS-VI.

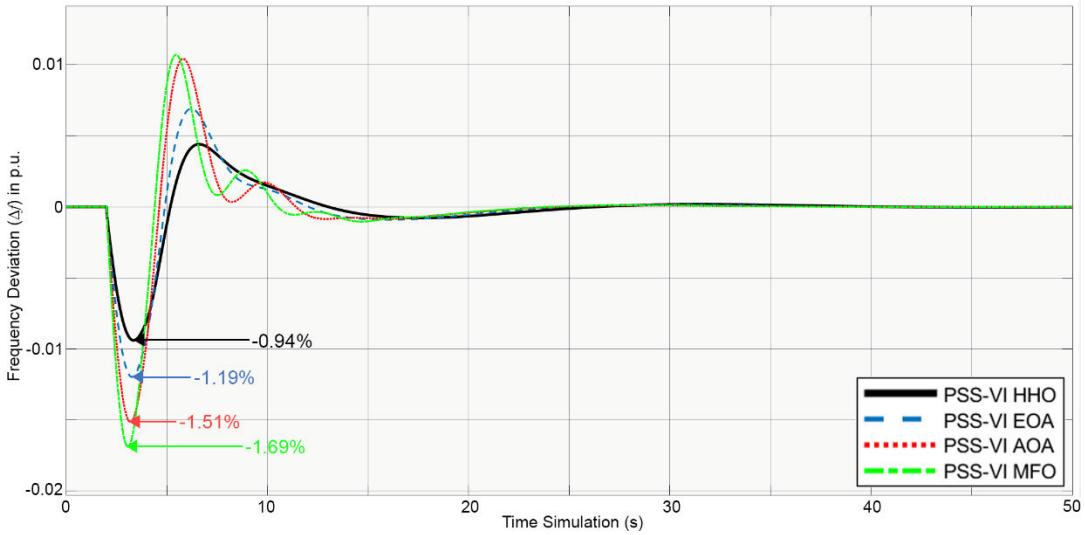

FIGURE 24. Δf_2 response in Case 3 Scenario 2 of hybrid controlling for PSS-VI.

and Scenario 2. The difference is the RES-level condition. In Scenario 1 (low-RES level condition), the proportion of RES power output is less than the conventional generators. Δf_1, Δf_2, and $\Delta P_{tie,21}$ responses in Scenario 1 are shown in Figure 20, Figure 21, and Figure 22, respectively. Besides that, a detailed response in statistics is presented in Table 12. The HHO has superior results based on RoCoF. In Δf_1, HHO gives the best RoCoF of -0.87%, which is followed by AOA, MFO, and EOA of -1.13%, - 1.14%, and -1.17%, respectively. In Δf_2, HHO also gives the best RoCoF of -0.95%, which is followed by EOA, AOA, and MFO of -1.12%, -1.4%, and -1.47%, respectively. In $\Delta P_{tie,21}$, the RoCoF is suppressed by HHO of $+0.31\%$, which is followed by EOA, AOA, and MFO of $+0.77\%$, $+1.03\%$, and $+1.12\%$, respectively.

In high-RES level conditions (Scenario 2), the Δf_1, Δf_2, and $\Delta P_{tie,21}$ has presented in Figure 23, Figure 24, and Figure 25, respectively. The detailed statistics of the responses are given in Table 13. In this scenario, HHO has also been successful in giving the highest suppression to the RoCoF. In Δf_1, HHO gives RoCoF of -0.94%, which is followed by EOA, MFO, and AOA of -1.01%, -1.07%, and -1.18%, respectively. In Δf_2, HHO offers a similar RoCoF of -0.94%, which is followed by EOA, AOA, and MFO of -1.19%, -1.51%, and -1.69%, respectively. Then, the RoCoF in $\Delta P_{tie,21}$ by HHO of $+0.37\%$, which is followed by EOA, AOA, and MFO of $+0.79\%$, $+1.09\%$, and $+1.89\%$, respectively.

The simulation in Case 3 shows that the hybrid controlling for PSS-VI by HHO can give better RoCoF suppression than

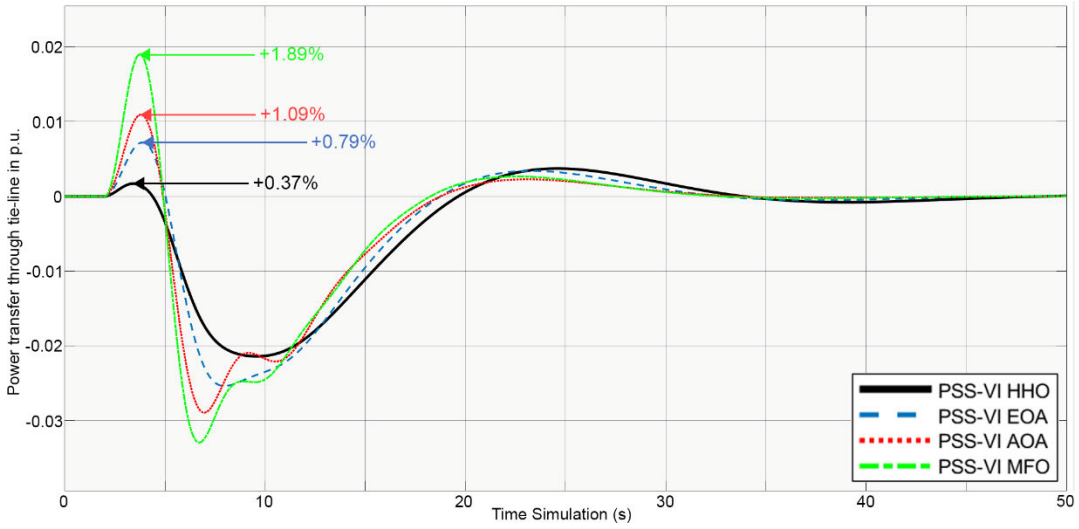

FIGURE 25. $\Delta P_{tie,12}$ response in Case 3 Scenario 2 of hybrid controlling for PSS-VI.

the others. The investigation results of the hybrid controlling parameters for PSS-VI in Case 3 have concluded that HHO offers a smoother response and transition in the oscillations.

V. CONCLUSION

The hybrid controlling parameters of PSS-VI using HHO in interconnected renewable power systems have been performed. The power systems have established different energy resources including conventional generators, SPG, WPG, and BSS to realize the virtual inertia emulation. This study was conducted by using a dynamic stability approach. Thus, the system and controllers were simplified based on the dynamic behavior of the system. It focused on small-signal oscillation due to small-signal disturbance. The small-signal disturbances have been simulated by small and sudden changes in power load, mechanical power, solar GHI, and wind speed. The experimental cases were carried out in MATLAB simulation.

The results of optimal parameters for PSS-VI show that HHO is superior in conducting the best fitness value compared to EOA, AOA, and MFO as the compared algorithms. Besides that, HHO has offered the fastest iterations than the others. Using eigenvalue analysis, the results in the hybrid controlling parameters for PSS-VI by algorithms are successful in shifting the eigenvalue point to the left. It indicated the proposed approach in this paper is suitable to enhance the stability. Moreover, HHO conducts the most negative value in all of the scenarios than the other algorithms that concluded HHO offers the best stability enhancement.

An in-depth analysis regarding the result of hybrid controlling parameters for PSS-VI is conducted using time domain simulation. In this analysis, various cases and scenarios are simulated to investigate the difference in working behavior in interconnected renewable power systems. The investigation has concluded that the hybrid controlling parameters for PSS-VI can enhance the stability of interconnected renewable power systems. HHO as a robust optimizer also can be adapted and outperform the compared algorithms in conducting the best enhancement effects in all of the cases. The results of hybrid controlling parameters by HHO can significantly suppress the Rate of Change of Frequency (RoCoF) to 0.18% to 5.99% in low-RES conditions and 0.11% to 4.89% in high-RES conditions. Moreover, the optimal parameters from HHO offer smoother oscillation and transition in frequency and inter-area power exchange responses.

In future works, further investigation for PSS-VI can be conducted with different approaches and algorithms. Besides that, the PSS-VI can be investigated in more complex models. Thus, the larger variation in small-signal disturbances, such as system faults and the fluctuations of natural conditions related to RES, can be considered.

ACKNOWLEDGMENT

The authors would like to be grateful to the Indonesian government for the PMDSU Batch VI and PKPI 2023 scholarship programs. This research was conducted in collaboration with the Power System Operation and Control (PSOC) Laboratory, Department of Electrical Engineering, Institut Teknologi Sepuluh Nopember (ITS) and Dr. Ryo Nishimura's Laboratory, Faculty of Engineering, Tottori University.

REFERENCES

[1] M. C. Brisbois, "Decentralised energy, decentralised accountability? Lessons on how to govern decentralised electricity transitions from multi-level natural resource governance," *Global Transitions*, vol. 2, pp. 16–25, Jan. 2020, doi: 10.1016/j.glt.2020.01.001.

[2] T. Wu, D.-L. Xu, and J.-B. Yang, "Decentralised energy and its performance assessment models," *Frontiers Eng. Manage.*, vol. 8, no. 2, pp. 183–198, Jun. 2021, doi: 10.1007/s42524-020-0148-7.

[3] J. Parra-Domínguez, E. Sánchez, and Á. Ordóñez, "The prosumer: A systematic review of the new paradigm in energy and sustainable development," *Sustainability*, vol. 15, no. 13, p. 10552, Jul. 2023, doi: 10.3390/su151310552.

[4] M. Uddin, H. Mo, D. Dong, S. Elsawah, J. Zhu, and J. M. Guerrero, "Microgrids: A review, outstanding issues and future trends," *Energy Strategy Rev.*, vol. 49, Sep. 2023, Art. no. 101127, doi: 10.1016/j.esr.2023.101127.
[5] M. H. Saeed, W. Fangzong, B. A. Kalwar, and S. Iqbal, "A review on Microgrids' challenges & perspectives," *IEEE Access*, vol. 9, pp. 166502–166517, 2021, doi: 10.1109/ACCESS.2021.3135083.
[6] J. Mitali, S. Dhinakaran, and A. A. Mohamad, "Energy storage systems: A review," *Energy Storage Saving*, vol. 1, no. 3, pp. 166–216, Sep. 2022, doi: 10.1016/j.enss.2022.07.002.
[7] Y. Yang, "Electricity interconnection with intermittent renewables," *J. Environ. Econ. Manage.*, vol. 113, May 2022, Art. no. 102653, doi: 10.1016/j.jeem.2022.102653.
[8] M. A. Prakasa and I. Robandi, "Optimal tuning for power system stabilizer using arithmetic optimizer algorithm in interconnected two-area power system," in *Proc. Int. Seminar Intell. Technol. Appl. (ISITIA)*, Jul. 2023, pp. 798–803, doi: 10.1109/ISITIA59021.2023.10221034.
[9] A. Behera, S. S. Pati, U. Subudhi, S. Ghatak, T. K. Panigrahi, M. H. Alsharif, and S. Mohsan, "Frequency stability analysis of multi-renewable source system with cascaded PDN-FOPI controller," *Sustainability*, vol. 14, no. 20, p. 13065, Oct. 2022, doi: 10.3390/su142013065.
[10] M. R. Djalal, I. Robandi, and M. A. Prakasa, "Stability enhancement of sulselrabar electricity system using mayfly algorithm based on static var compensator and multi-band power system stabilizer PSS2B," *IEEE Access*, vol. 11, pp. 57319–57340, 2023, doi: 10.1109/ACCESS.2023.3283598.
[11] J. Machowski, Z. Lubosny, J. Bialek, and J. Bumby, *Power System Dynamics: Stability and Control*. Hoboken, NJ, USA: Wiley, 2020.
[12] M. Shafiullah, M. J. Rana, M. S. Shahriar, and M. H. Zahir, "Low-frequency oscillation damping in the electric network through the optimal design of UPFC coordinated PSS employing MGGP," *Measurement*, vol. 138, pp. 118–131, May 2019, doi: 10.1016/j.measurement.2019.02.026.
[13] A. Nocoń and S. Paszek, "A comprehensive review of power system stabilizers," *Energies*, vol. 16, no. 4, p. 1945, Feb. 2023, doi: 10.3390/en16041945.
[14] P. Gupta, A. Pal, and V. Vittal, "Coordinated wide-area damping control using deep neural networks and reinforcement learning," *IEEE Trans. Power Syst.*, vol. 37, no. 1, pp. 365–376, Jan. 2022, doi: 10.1109/TPWRS.2021.3091940.
[15] P. He, Q. Fang, H. Jin, Y. Ji, Z. Gong, and J. Dong, "Coordinated design of PSS and STATCOM-POD based on the GA-PSO algorithm to improve the stability of wind-PV-thermal-bundled power system," *Int. J. Electr. Power Energy Syst.*, vol. 141, Oct. 2022, Art. no. 108208, doi: 10.1016/j.ijepes.2022.108208.
[16] J. Ansari, A. R. Abbasi, M. H. Heydari, and Z. Avazzadeh, "Simultaneous design of fuzzy PSS and fuzzy STATCOM controllers for power system stability enhancement," *Alexandria Eng. J.*, vol. 61, no. 4, pp. 2841–2850, Apr. 2022, doi: 10.1016/j.aej.2021.08.007.
[17] M. Erdiwansyah, H. Husin, Nasaruddin, M. Zaki, and Muhibbuddin, "A critical review of the integration of renewable energy sources with various technologies," *Protection Control Mod. Power Syst.*, vol. 3, no. 3, Feb. 2021, doi: 10.1186/s41601-021-00181-3.
[18] T. Kerdphol, F. S. Rahman, M. Watanabe, and Y. Mitani, *Virtual Inertia Synthesis and Control*. Springer, 2021. [Online]. Available: https://link.springer.com/book/10.1007/978-3-030-57961-6
[19] A. Pratap, S. K. Sharma, and A. Khandelwal, "A review of modern virtual inertia control strategies for microgrid implementation," in *Proc. IEEE 2nd Int. Conf. Electr. Power Energy Syst. (ICEPES)*, Dec. 2021, pp. 1–6, doi: 10.1109/ICEPES52894.2021.9699804.
[20] K. Y. Yap, C. R. Sarimuthu, and J. M.-Y. Lim, "Virtual inertia-based inverters for mitigating frequency instability in grid-connected renewable energy system: A review," *Appl. Sci.*, vol. 9, no. 24, p. 5300, Dec. 2019.
[21] A. Faragalla, O. Abdel-Rahim, M. Orabi, and E. H. Abdelhameed, "Enhanced virtual inertia control for microgrids with high-penetration renewables based on whale optimization," *Energies*, vol. 15, no. 23, p. 9254, Dec. 2022, doi: 10.3390/en15239254.
[22] L. Carvalho, J. R. L. Neto, J. C. Rezende, M. V. S. Costa, E. V. Fortes, and L. H. Macedo, "Linear quadratic regulator design via metaheuristics applied to the damping of low-frequency oscillations in power systems," *ISA Trans.*, vol. 134, pp. 322–335, Mar. 2023, doi: 10.1016/j.isatra.2022.08.024.
[23] T. Kerdphol, F. S. Rahman, M. Watanabe, Y. Mitani, D. Turschner, and H.-P. Beck, "Enhanced virtual inertia control based on derivative technique to emulate simultaneous inertia and damping properties for microgrid frequency regulation," *IEEE Access*, vol. 7, pp. 14422–14433, 2019, doi: 10.1109/ACCESS.2019.2892747.
[24] T. Kerdphol, F. S. Rahman, Y. Mitani, M. Watanabe, and S. K. Küfeoğlu, "Robust virtual inertia control of an islanded microgrid considering high penetration of renewable energy," *IEEE Access*, vol. 6, pp. 625–636, 2018, doi: 10.1109/ACCESS.2017.2773486.
[25] Q. Li, B. Ren, Q. Li, D. Wang, W. Tang, J. Meng, and X. Wu, "Virtual inertial control strategy based on fuzzy logic algorithm for PMSG wind turbines to enhance frequency stability," *Frontiers Energy Res.*, vol. 10, pp. 1–9, May 2022, doi: 10.3389/fenrg.2022.907770.
[26] V. Skiparev, J. Belikov, E. Petlenkov, and Y. Levron, "Reinforcement learning based MIMO controller for virtual inertia control in isolated microgrids," in *Proc. IEEE PES Innov. Smart Grid Technol. Conf. Eur. (ISGT-Europe)*, Oct. 2022, pp. 1–5, doi: 10.1109/ISGT-Europe54678.2022.9960447.
[27] B. N. Syifa, D. A. Asfani, A. Priyadi, and H. Setiadi, "Frequency stability analysis on optimization of virtual inertia controller settings based on retired electric vehicles battery using firefly algorithm," in *Proc. Int. Conf. Comput. Eng., Netw., Intell. Multimedia (CENIM)*, Nov. 2022, pp. 1–6, doi: 10.1109/CENIM56801.2022.10037414.
[28] A. N. A. Maulidhia, D. A. Asfani, A. Priyadi, and H. Setiadi, "Frequency stability analysis on optimization of virtual inertia control (VIC) capacitor energy storage (CES) controller settings using particle swarm optimization," in *Proc. Int. Conf. Comput. Eng., Netw., Intell. Multimedia (CENIM)*, Nov. 2022, pp. 359–364, doi: 10.1109/CENIM56801.2022.10037313.
[29] E. V. Fortes, B. Martins, M. V. S. Costa, L. Carvalho, and L. H. Macedo, "Mayfly optimization algorithm applied to the design of PSS and SSSC-POD controllers for damping low-frequency oscillations in power systems," *Int. Trans. Elect. Energy Syst.*, vol. 2022, Apr. 2022, Art. no. 5612334.
[30] A. T. Moghadam, M. Aghahadi, M. Eslami, S. Rashidi, B. Arandian, and S. Nikolovski, "Adaptive rat swarm optimization for optimum tuning of SVC and PSS in a power system," *Int. Trans. Elect. Energy Syst.*, vol. 2022, Jan. 2022, Art. no. 4798029, doi: 10.1155/2022/4798029.
[31] M. A. Prakasa, I. Robandi, R. Nishimura, and M. R. Djalal, "A new scheme of Harris hawk optimizer with memory saving strategy (HHO-MSS) for controlling parameters of power system stabilizer and virtual inertia in renewable microgrid power system," *IEEE Access*, early access, 2024, doi: 10.1109/ACCESS.2024.3385089.
[32] W. Gil-González, O. D. Montoya, A. Escobar-Mejía, and J. C. Hernández, "LQR-based adaptive virtual inertia for grid integration of wind energy conversion system based on synchronverter model," *Electronics*, vol. 10, no. 9, p. 1022, Apr. 2021.
[33] E. Rakhshani, I. M. H. Naveh, H. Mehrjerdi, and K. Pan, "An optimized LQG servo controller design using LQI tracker for VSP-based AC/DC interconnected systems," *Int. J. Electr. Power Energy Syst.*, vol. 129, Jul. 2021, Art. no. 106752, doi: 10.1016/j.ijepes.2020.106752.
[34] A. Mešanović, U. Münz, A. Szabo, M. Mangold, J. Bamberger, M. Metzger, C. Heyde, R. Krebs, and R. Findeisen, "Structured controller parameter tuning for power systems," *Control Eng. Pract.*, vol. 101, Aug. 2020, Art. no. 104490, doi: 10.1016/j.conengprac.2020.104490.
[35] P. Sarajcev, A. Kunac, G. Petrovic, and M. Despalatovic, "Artificial intelligence techniques for power system transient stability assessment," *Energies*, vol. 15, no. 2, p. 507, Jan. 2022.
[36] A. Saleh, W. A. Omran, H. M. Hasanien, M. Tostado-Véliz, A. Alkuhayli, and F. Jurado, "Manta ray foraging optimization for the virtual inertia control of islanded microgrids including renewable energy sources," *Sustainability*, vol. 14, no. 7, p. 4189, Apr. 2022, doi: 10.3390/su14074189.
[37] M. A. Prakasa and I. Robandi, "Power system stabilizer tuning improvement for single-machine infinite bus using equilibrium optimizer algorithm," in *Proc. Int. Seminar Intell. Technol. Appl. (ISITIA)*, Jul. 2022, pp. 320–325, doi: 10.1109/ISITIA56226.2022.9855203.
[38] I. Boucetta, D. Naimi, A. Salhi, S. Abujarad, and L. Zellouma, "Power system stability enhancement using a novel hybrid algorithm based on the water cycle moth-flame optimization," *Energies*, vol. 15, no. 14, p. 5060, Jul. 2022.
[39] M. A. Prakasa and I. Robandi, "Tuning improvement of power system stabilizer using hybrid Harris hawk optimization-equilibrium optimizer algorithm," in *Proc. 6th Int. Conf. Inf. Technol., Inf. Syst. Electr. Eng. (ICITISEE)*, Dec. 2022, pp. 553–558.

[40] A. A. Heidari, S. Mirjalili, H. Faris, I. Aljarah, M. Mafarja, and H. Chen, "Harris hawks optimization: Algorithm and applications," *Future Gener. Comput. Syst.*, vol. 97, pp. 849–872, Aug. 2019, doi: 10.1016/j.future.2019.02.028.
[41] B. K. Tripathy, P. K. R. Maddikunta, Q. V. Pham, T. R. Gadekallu, K. Dev, S. Pandya, and B. M. ElHalawany, "Harris hawk optimization: A survey onvariants and applications," *Comput. Intell. Neurosci.*, vol. 2022, Jun. 2022, Art. no. 2218594, doi: 10.1155/2022/2218594.
[42] M. Shehab, I. Mashal, Z. Momani, M. K. Y. Shambour, A. Al-Badareen, S. Al-Dabet, N. Bataina, A. R. Alsoud, and L. Abualigah, "Harris hawks optimization algorithm: Variants and applications," *Arch. Comput. Methods Eng.*, vol. 29, no. 7, pp. 5579–5603, Nov. 2022, doi: 10.1007/s11831-022-09780-1.
[43] M. A. El-Dabah, M. H. Hassan, S. Kamel, and H. M. Zawbaa, "Robust parameters tuning of different power system stabilizers using a quantum artificial gorilla troops optimizer," *IEEE Access*, vol. 10, pp. 82560–82579, 2022, doi: 10.1109/ACCESS.2022.3195892.
[44] S. R. Paital, P. K. Ray, A. Mohanty, and S. Dash, "Stability improvement in solar PV integrated power system using quasi-differential search optimized SVC controller," *Optik*, vol. 170, pp. 420–430, Oct. 2018, doi: 10.1016/j.ijleo.2018.05.097.
[45] D.-J. Lee and L. Wang, "Small-signal stability analysis of an autonomous hybrid renewable energy power generation/energy storage system Part I: Time-domain simulations," *IEEE Trans. Energy Convers.*, vol. 23, no. 1, pp. 311–320, Mar. 2008, doi: 10.1109/TEC.2007.914309.
[46] *IEEE Recommended Practice for Excitation System Models for Power System Stability Studies*, IEEE, New York, NY, USA, Aug. 2016, doi: 10.1109/IEEESTD.2016.7553421.
[47] T. Kerdphol, F. S. Rahman, V. Phunpeng, M. Watanabe, and Y. Mitani, "Demonstration of virtual inertia emulation using energy storage systems to support community-based high renewable energy penetration," in *Proc. IEEE Global Humanitarian Technol. Conf. (GHTC)*, Oct. 2018, pp. 1–7, doi: 10.1109/GHTC.2018.8601755.
[48] P. S. Kundur and O. P. Malik, *Power System Stability and Control*, 2nd ed. New York, NY, USA: McGraw-Hill, 2020.
[49] H. M. Alabool, D. Alarabiat, L. Abualigah, and A. A. Heidari, "Harris hawks optimization: A comprehensive review of recent variants and applications," *Neural Comput. Appl.*, vol. 33, no. 15, pp. 8939–8980, 2021, doi: 10.1007/s00521-021-05720-5.
[50] M. Chawla and M. Duhan, "Levy flights in metaheuristics optimization algorithms—A review," *Appl. Artif. Intell.*, vol. 32, nos. 9–10, pp. 802–821, 2018, doi: 10.1080/08839514.2018.1508807.
[51] A. Faramarzi, M. Heidarinejad, B. Stephens, and S. Mirjalili, "Equilibrium optimizer: A novel optimization algorithm," *Knowl.-Based Syst.*, vol. 191, Mar. 2020, Art. no. 105190, doi: 10.1016/j.knosys.2019.105190.
[52] L. Abualigah, A. Diabat, S. Mirjalili, M. Abd Elaziz, and A. H. Gandomi, "The arithmetic optimization algorithm," *Comput. Methods Appl. Mech. Eng.*, vol. 376, Apr. 2021, Art. no. 113609, doi: 10.1016/j.cma.2020.113609.
[53] S. Mirjalili, "Moth-flame optimization algorithm: A novel nature-inspired heuristic paradigm," *Knowl.-Based Syst.*, vol. 89, pp. 228–249, Nov. 2015, doi: 10.1016/j.knosys.2015.07.006.

MOHAMAD ALMAS PRAKASA was born in Brebes, in September 1999. He received the bachelor's degree from the Department of Electrical Engineering, Universitas Negeri Semarang (UNNES), Semarang, Indonesia, in 2017, the master's degree from the Department of Electrical Engineering, Institut Teknologi Sepuluh Nopember (ITS), Surabaya, Indonesia, in 2021, where he is currently pursuing the Ph.D. degree. He is a member of the Power System Operation and Control (PSOC) Laboratory. His master's and Ph.D. degrees were supported by the Fast-Track Scholarship Program from the Republic of Indonesia and the PMDSU Scholarship Program. His research interests include artificial intelligence application to electrical power systems, especially to dynamic stability and RES microgrid optimization.

IMAM ROBANDI was born in Kebumen, in August 1963. He received the bachelor's degree from the Department of Electrical Engineering, Institut Teknologi Sepuluh Nopember (ITS), Surabaya, Indonesia, in 1989, the master's degree from the Department of Electrical Engineering, Institut Teknologi Bandung (ITB), Bandung, Indonesia, in 1995, and the Ph.D. degree from the Department of Electrical Engineering, Tottori University, Japan, in 2002. He is currently a Professor with the Department of Electrical Engineering, ITS. He is also the Head of the Power System Operation and Control (PSOC) Laboratory. His expertise and specialization in research are the artificial intelligence applications for large-scale electrical and energy power systems.

RYO NISHIMURA was born in Sapporo, Japan, in July 1966. He received the bachelor's, master's, and Ph.D. degrees from the Department of Nuclear Engineering, Hokkaido University, Japan, in 1989, 1991, and 1994, respectively. He is currently an Associate Professor with the Department of Electrical Engineering and Computer Science, Tottori University. His research interests include heuristic algorithms, PV power generation, and the application of electrostatics.

MUHAMMAD RUSWANDI DJALAL was born in Makassar, Indonesia, in March 1990. He received the bachelor's degree in energy engineering from Politeknik Negeri Ujung Pandang, Makassar, in 2012, and the master's degree from the Department of Electrical Engineering, Institut Teknologi Sepuluh Nopember (ITS), Surabaya, Indonesia, in 2015, where he is currently pursuing the Ph.D. degree. He is a Lecturer in energy engineering with the Department of Mechanical Engineering, Politeknik Negeri Ujung Pandang. His research interests include power system stability, renewable energy, and artificial intelligence.